TOWARD BETTER UNDERSTANDING OF MECHANICAL RESPONSE OF FABRICS UNDER MULTIPLE COMBINED LOADING MODES: EXPERIMENTAL AND STATISTICAL ANALYSIS

by

Samia Sultana Mir

B.Sc. Bangladesh University of Engineering and Technology, Bangladesh, 2012

A THESIS SUBMITTED IN PARTIAL FULFILLMENT
OF THE REQUIREMENTS FOR THE DEGREE OF

MASTER OF APPLIED SCIENCE

in

The College of Graduate Studies
(Mechanical Engineering)

THE UNIVERSITY OF BRITISH COLUMBIA

(Okanagan)

August 2015

Abstract

Fabric reinforced composites are becoming among primary materials of choice in manufacturing damage tolerant aerospace, automotive, and naval architectural parts. Detailed characterization of fabric reinforcements, however, is necessary to ensure the quality of such composite part and to prevent structural failure during their service. A number of experimental studies have been dedicated in the past to characterize the deformation of fabrics under individual loading modes, such as pure uniaxial tension, pure biaxial tension and pure shear. There still exists, however, a lack of knowledge and standardization in testing and analyzing the mechanical response of fabrics under combined shear-tension loadings, both in simultaneous and sequential modes. Moreover, in reality, there are sources of uncertainties in the forming of these multi-scale fibrous materials, which often results in non-repeatable test data and causes inconsistencies for full characterization.

Recognizing the above gaps, the aim of this thesis has been to design, conduct, and analyze a set of experiments for enhanced characterization of a typical glass fabric under select individual and combined shear-biaxial tension loading modes. The experimental tests were performed using a new fixture recently designed and manufactured by the Composites & Optimization Laboratory at UBC and its international partners. On the account of inherent material uncertainties, all tested deformation modes were analyzed and compared via a series of ANOVA analysis. Results showed that statistically there were significant differences between the warp and weft responses of the fabric under all the deformation modes, with weft yarns being generally stiffer. The shear-tension coupling effect in combined deformation modes yielded

higher normal axial and shear forces compared to the individual deformation modes. More severe local damage zones were observed during the coupling tests. Finally, a Digital Image Correlation test was conducted to inspect wrinkling in the deformed specimens. Under a pure shear mode, some out of plane wrinkles appeared due to misalignment, whereas in the simultaneous loading condition it was nearly disappeared, thanks to the presence of fiber tension.

Preface

This thesis presents an experimental-statistical analysis of shear/tension response of fabrics which was conducted in the Composites & Optimization Laboratory at the School of Engineering, University of British Columbia-Okanagan. The thesis has been supervised by Dr. Abbas S. Milani. Part of the thesis was published as two conference posters as follows.

- Rashidi, S. Sultana, B. Crawford, M. DeWachter, A. S. Milani (2015) "Towards wrinkling-free forming of woven composite materials", 2nd Annual Engineering Graduate Symposium, June 8th, 2015, School of Engineering, UBC Okanagan (awarded the best MASc poster presentation)
- Samia Sultana Mir, A. S. Milani (2014) "Woven fabrics characterization under combined loading", 1st Annual Engineering Graduate Symposium, May 1, 2014, School of Engineering, UBC Okanagan

Chapters 2-4 will be submitted soon for possible publications. The thesis contribution relies on enhancing a novel experimental set-up for biaxial-shear characterization of fabrics, along with adapting a new statistical framework for comparing the mechanical response of yarns in these reinforcing materials within and between deformation modes.

Table of Contents

List of Tables

List of Figures

List of Abbreviations

CRN	Composites Research Network
CS	Circular shear
DIC	Digital Image Correlation
PF	Picture Frame
BE	Bias-Extension
DSFM	Direct Shear Force Measurement
LVDT	Linear variable differential transducers
CF	Coupling Factor

Glossary of Notation

F_{sh}	Shear force
d_{sh}	Shear displacement
L_{frame}	Picture frame length
A_{sh}	Fabric area
γ	Shear angle
θ	Angle of picture frame
F_{crit}	Critical value of F statistics
P	Probability for rejecting null hypothesis
H_o	Null hypothesis
H_1	Alternative hypothesis
μ	Mean of material response

Acknowledgements

I would like to thank my supervisor Dr. Abbas S. Milani who provided me the opportunity to work on a cutting-edge research area related to characterization of fabric composites. Also, his guidance and support helped me achieve my research goals methodically and enjoyably.

I would like to thank the members of my thesis supervisory committee, Dr. Bahman Naser and Dr. Shahria Alam, for their valuable time and encouragements.

This thesis would not be easy without the generous help and efforts of Dr. Mohammad Nouroz Islam at the Composites & Optimization Laboratory. I have learned from him how to operate and program the LabView software, how to perform LVDT set-ups and design optimized fabric clamping systems. I would like to acknowledge the Laboratory Coordinator Mr. Bryn James Crawford, who always helped me to deal with challenging experimental set-ups and provided valuable suggestions. I am thankful to my friends Mr. Juan David Torres Forero and Mr. Masoud Haghi Kashani for their assistance during the Digital image correlation analysis. I am very grateful to my friend Dr. Mojtaba Komeili for his help at the initial stages of my acquaintance with the magnificent field composites.

My heartiest gratitude goes to my parents who sacrificed a lot to make their daughter an engineer and always providing unconditional love. I would also like to acknowledge my lovely sister, Sabiha Sultana Mir and my brother, Md. Samiur Rahman Mir for their support from a distant place. My deepest gratitude goes to my mother in law for her love and care from thousands miles away, which provided me a big support during my MASc studies.

Finally, and above all, thanks to my dear husband Mr. Mohammad Mamunur Rahman for his constant care, support, sacrifice and appreciation throughout my graduate studies.

Dedication

This thesis is dedicated to my ever caring parents:

Md. Abdur Razzak Mir

&

Tahura Sultana

Chapter 1: Background and Thesis Organization

1.1 Introduction

Dry fabrics have already received a considerable attention from industries and researchers for their promising applications in aerospace, automobile, and naval structures. Over the past decade, a large portion of the studies in the composite materials field has been dedicated to fabrics to predict their mechanical behavior under different forming conditions, along with undesired defects such as wrinkling that if controlled, can significantly improve the quality of final products. The present research work is based on an enhanced experimental characterization and statistical analysis of dry fabrics. This chapter covers the motivation and objective of the study and includes the thesis outline.

1.2 Problem definition and motivation

Fabric reinforced composites have gained attention by several industrial sectors for their low cost and superior multi-axial properties, along with ease of forming process. However, complexities can arise during the manufacturing of fabric composites such as wrinkling and fiber waviness/ misalignment, which in turn can affect the effective properties of the final products (Mesogitis et al., 2014). Sheahan (2015) studied keel failures in race boats and reported that from 1984 to 2015, 72 cases have been found under such failure instant, causing a total loss of 24 lives. As another example, the National Transportation Safety Board reported on 1 April, 2011 about the Boeing 737-3H4 which faced a quick decompression during service (Hersman, 2013). The investigation suggested that the fuselage crown skin installation/manufacturing may not have been accurate (Hersman, 2013). As part of improving the quality of such high-risk composite structures, it is important to avoid catastrophic failures in their reinforcement agents, while

lowering manufacturing complexities during the production of multifaceted 3D shapes. This is the reason for which some researchers have paid close attention in recent years to accurate mechanical characterization of fiber fabrics as a promising reinforcement architecture type for damage tolerant composite structures (Cao et al., 2008; Mesogitis et al., 2014; Smith & Vaidya, 2013; Taha et al., 2013; Zhu et al., 2007). A large number of experiments and simulations among the past works have been carried out particularly on basic deformation modes such as pure tension and/or pure shear of dry fabrics (Cao et al., 2008; Flores-Johnson et al., 2014; Willemset al., 2008; Yin et al., 2014). However, there is much less information on biaxial behavior of fabrics (Chen et al., 2011; Jackson et al., 2010). Likewise, simultaneous biaxial tension-shear (combined) testing of fabrics has received attention only recently (Chen et al., 2011; Jackson et al., 2010; Nosrat-Nezamiet al., 2014). Before curing of dry fabrics, they are often considered as meso or micro-level material systems and after curing, the composite parts are considered as macro level systems. To better understand fabrics' draping behavior and to avoid potential local defects such as wrinkling, it is critical to characterize their tension-shear coupling effects at a meso-level. As a result, next to experimental work above, efforts have been made to numerically study the tension-shear behavior of fabrics (Harrison, 2012; Lee et al., 2009; Lee et al., 2010). Overall, the majority of the above studies have not reported/compared other types of simultaneous loadings such as sequential trellising shear-biaxial tension or sequential biaxial tension-trellising shear, nor showed the coupling effect under circular/sliding shear mode. In addition, no study has incorporated a full statistical analysis framework to reliably characterize the variation in fabrics' tests under different loading directions and different modes. The latter two gaps in knowledge formed the motivation of the present work.

The experimental part of the research has employed a new biaxial tension-shear loading machine (Figure 1.1) that was collaboratively designed and manufactured by the City College of New York (CCNY), Naval Undersea Warfare Center (NUWC), and the Composites & Optimization Group at UBC Okanagan.

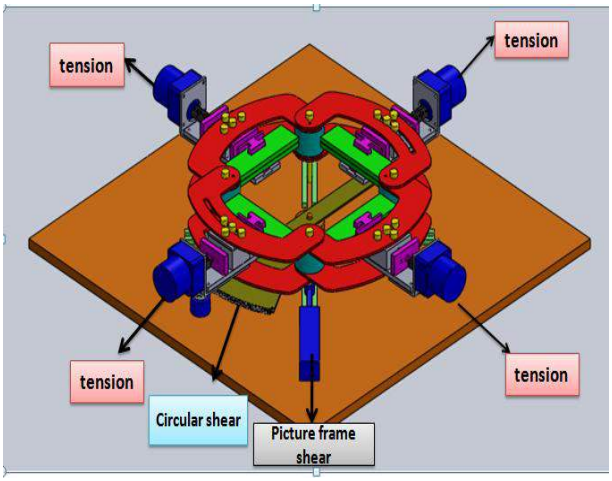

Figure 1.1: Schematic of a biaxial-shear test fixture used in this thesis (Elliot et al. 2012).

1.3 Objectives of the study

This study's general objective is to enhance our understanding of complex behavior of fabrics under different deformation modes, through an integrated experimental-statistical analysis. The specific objectives include:

1. Characterization of a Fiberglass non crimp fabric under a series of single and combined deformation modes (quasi-static rate).
2. Statistical analysis of data and tension-shear coupling effects in the fabric.
3. Preliminary recommendations to avoid wrinkling via tension-assisted draping.

1.4 Thesis outline

Chapter 1 described the objective and motivation of the study and gave a general introduction to biaxial-shear fabric testing approach. Chapter 2 includes a literature review on fabric materials characterization, where a number of earlier researches are discussed and compared. Chapter 3 provides the methodology used in the current research, along with the description of the biaxial-shear fixture set-up. Chapter 4 presents and discusses the results obtained throughout the tests. In addition, the same chapter discusses the results of statistical analysis on test data under different deformation modes. Finally, Chapter 5 includes the main conclusions of the work and outlines a potential future work direction.

Chapter 2: Literature Review

This chapter includes a literature review of past researches on dry fabric materials. This also includes fibers in composites manufacturing processes and challenges, dry fabric characterization and combined loading phenomenon.

2.1 Fiber reinforced composites

Fibers in a composite material are surrounded by a matrix material and the percentage of fiber-matrix combination contributes to the effective properties of the final consolidated material system. Among different types of composites, fiber reinforced polymer composites has perhaps presented the most benefit to leading industries such as aerospace and automotive, thanks to their superior mechanical properties combined with ease of manufacturing and relatively low cost. Evidenced by Mir and her peers (2015; 2012; 2013), in order to further maximize this benefit over a range of fiber reinforcements and polymer matrix types, researchers have widely improved the fiber-matrix compatibilities as well as their adhesions by treating the reinforced fibers and also introducing new forms of fibrous reinforcement architectures.

2.2 Dry fabrics: application and manufacturing

Among different types of fibrous reinforcement architectures, woven fabrics are formed by weaving of warp and weft yarns into one another. Another kind of dry reinforcements is known as non-crimp fabrics. Both of these materials have a sheet or mat-like shape and the fabric reinforcement is composed of thousand threads of fibers made of, e. g., carbon, glass, aramid, etc. (Launay et al., 2008). In the case of woven fabrics, the material properties are closely dependent on the weaving type and direction. Woven fabrics are often classified based on their weaving types like plain weave, twill weave, satin weave, basket weave, leno weave and mock leno weave (Strong, 2008). On the other hand, non-crimp fabrics are sheet or web structures

comprised of chopped or long fibers consolidated by bonds of a different nature than weaving (e. g., chemical, stitching, thermal, etc) and are generally known to offer better handling and mechanical properties in specific applications due to the absence of crimp (Edgren et al., 2004; Creech & Pickett 2006). in either case, dry fabrics (i. e., before consolidation with matrix) are considered as micro/meso structures, properties of which can directly affect the quality and properties of the final consolidated part at macro-level (Guagliano & Riva, 2001).

Due to the high drapability of fabrics, they are capable of preforming into three dimensional shapes, before consolidating/curing with a resin. To manufacture fabric reinforced composites, the consolidation is done, e. g., by means of resin transfer molding (RTM), resin injection molding (RIM), filament winding and fabric performing (Cao et al., 2008; Stig, 2008; Rowell et al., 1997). After 1997, some researches also explored the use of thermo-stamping (Sargent et al., 2010) and hydro-forming (Yuet al., 2003; Zampaloni et al., 2004) to manufacture fabric composites (Abdiwi at al., 2013; Stig, 2009). Large components in today's composite industries are, for the most part, made by hand lay-up (Sabbagh & Taha, 2013; Gujjala et al., 2014; Patel et al., 2011), press-molding (Sabbagh & Taha, 2013; Ray et al., 2007) and resin-transfer molding (Sabbagh & Taha, 2013; Rowell et al., 1997).

Next to low manufacturing costs, high impact tolerance, high specific stiffness and strength, there are other advantages of woven/non-woven fabrics for industrial applications. For example, owing to non magnetic properties and low weights, these composites are highly used in naval vessels and high speed crafts (Hayman et al., 2001). In fact, fiber reinforced composites have been used in the field of naval architecture since 1960 and lately they are receiving attention in modern naval structures such as Norwegian prototype surface effect ship 'Skjold' and French La

Fayette class Frigates(Hayman et al., 2001). Other examples of commercial applications of fabrics include energy absorption products (e. g., Helmet) (Cao et al., 2008; Yuet al., 2000), aerospace and defense (e. g., engine inlet cowlings, fuselage sections, rotor blade spars and fuel pods) (Cao et al., 2008; Rudd et al., 1999), automotive and associated applications (e. g., battery trays, seat structures, front end modules and load floors) (Cao et al., 2008; Long et al., 2001).

2.3 Composite manufacturing challenges

Although application of composites have been and continue to be of high interest to several industries, there are defects during manufacturing/application of these materials which occasionally create difficulties and challenges to designers. As an example, Hayman and his peers worked on a project on the use of fiber reinforced composites in naval ships and their report showed that air blast, under water shock and impact loads are some of the challenges for composite naval architectures (Hayman et al., 2001). A number of aerospace, automobile, sport goods etc. manufacturers are facing similar challenges during manufacturing of composites (Conor et al., 2012; Hayman et al., 2001). Mesogitis and his peers summarized (Figure 2.1) several types of uncertainties that may be encountered during composites manufacturing processes (Mesogitis et al., 2014).

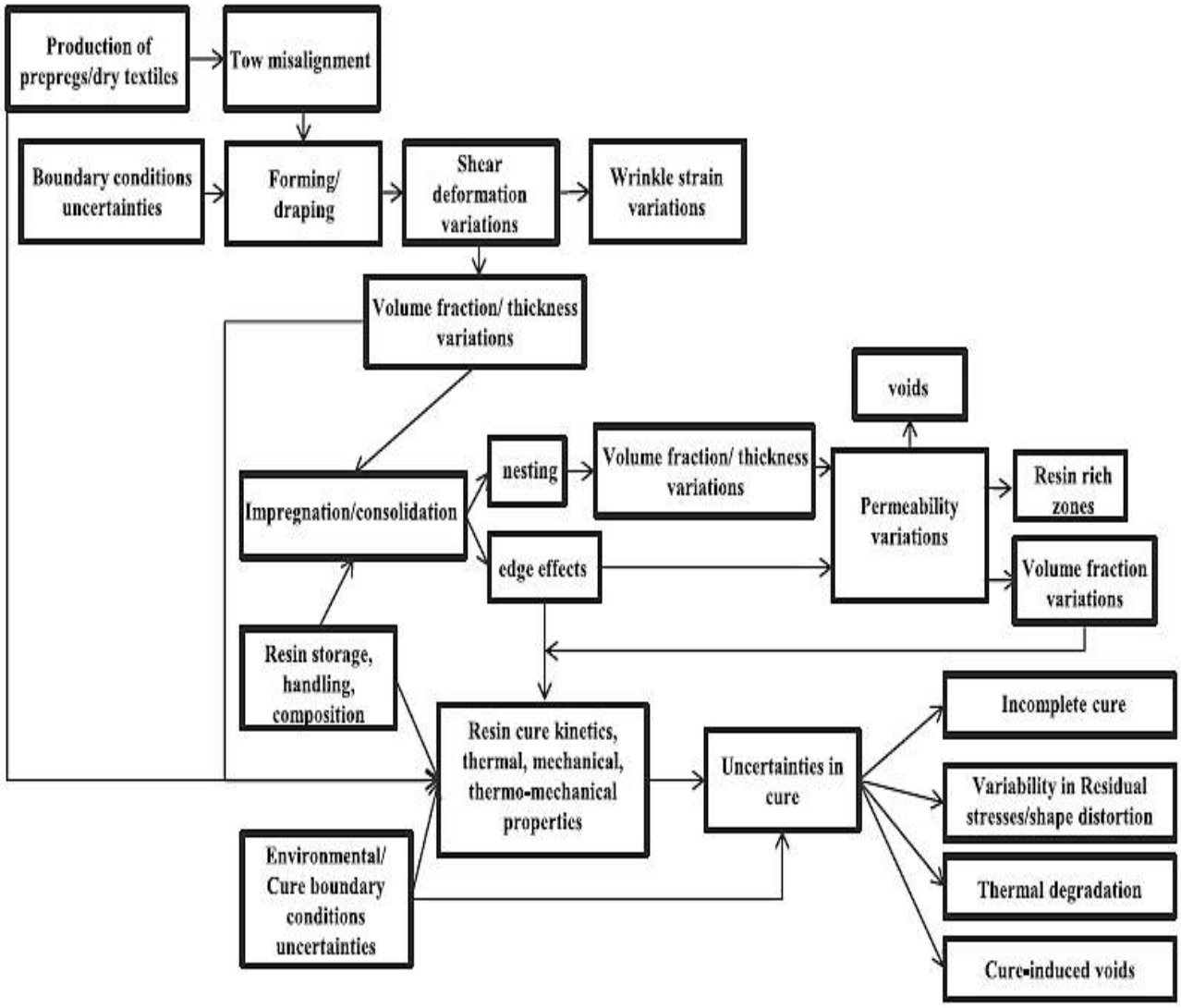

Figure 2.1: Overview of challenges in composites manufacturing with prepregs /dry textile reinforcements (Mesogitis et al., 2014).

During draping and consolidation of fabrics onto double curved shapes, void formation, nesting, residual stress formation, delamination, crack initiation and shape distortions are among common types of observed defects (Boisse et al., 2011). As per (Collier, 1991), a fabric's capacity to structure folds when it is bowed under its own particular weight may be characterized as draping. Sabbagh and Taha worked with jute woven fabrics to determine the feasibility of this type of fabric in place of Fiberglass fabric using a drape meter. They particularly measured the drape

coefficient and concluded that a low drape coefficient suggests better deformation, though an increment in the coefficient suggested a more hardened fiber that is less vulnerable against deformity (Sabbagh & Taha, 2013).

Sabbagh and Taha also suggested that the draping behavior of fabrics assumes an imperative part in esthetics, and also the acknowledgment of the final development and fiber permeability, wettability, and resin absorption all closely depend on draping behavior of material (Sabbagh & Taha, 2013). Particularly for resin-transfer molding techniques, it has been reported that the inhomogeneity of fiber volume fraction all through the part as well as changes in fiber orientation can take place during draping and consolidation (Fong & Advani, 1994). As indicated by other researchers, these issues tend to be even more evident when working with non-woven fabrics and natural strands (Sabbagh & Taha, 2013; Hancock & Potter, 2006).

Among different types of major defects during fabric composite manufacturing, wrinkling and misalignment are further discussed in the following sections, as they are related to the subsequent characterization tests in this thesis.

2.3.1 Out of plane wrinkle

Aerospace and automotive industries frequently follow resin transfer molding (RTM) process to manufacture composite parts where the reinforcement fabric is laid on the forming mold and after that resin is infused, followed by curing process (Lightfoot et al., 2013a). The targeted composite parts should be free from defects, but unfortunately out of plane wrinkling sometimes occurs during molding stages, which in turn can lower the mechanical property of the final part (Bloom et al., 2013; Hayman, et al., 2007; Hsiao & Daniel, 1996; Lightfoot et al., 2013a). In

order to increase the final composite parts' quality and to lower the part design cost, manufacturers should possess a good understanding of wrinkling sources (Zhu et al, 2008). Wrinkling forms basically by an entire re-arrangement of strains, stiffness, and boundary conditions in the fabric (Sabbagh & Taha, 2013). In practice, when fabrics are consolidated into a curved mold, such as a U shape, there is a possibility of ply slippage during consolidation, which can lead to wrinkles (Figure 2.2) (Lightfoot et al., 2013a; Lightfoot et al., 2013h). Additionally, researchers have shown that the mismatch of coefficient of thermal expansion between the tool and fabric material can lead to wrinkling (Çınar & Ersoy, 2015; Lightfoot et al., 2013).

Figure 2.2: Formation of wrinkles in consolidation stage of a fabric into a curved mold (Lightfoot et al., 2013a).

2.3.2 Misalignment of yarns

A recent work has shown that misalignment of woven fabrics can depend on the warp and weft yarn orientations while laying up the plies (Lightfoot et al., 2013a). Misalignment is a very common behavior for dry fabrics as they are naturally loose and packaged in roll form, where the warp and weft may not always become perfectly aligned. In Figure 2.3, the red, green, blue and magenta highlighted lines indicate waviness in a sheared fabric, in the range of $\pm 8^0$ (Lightfoot et al., 2013a).

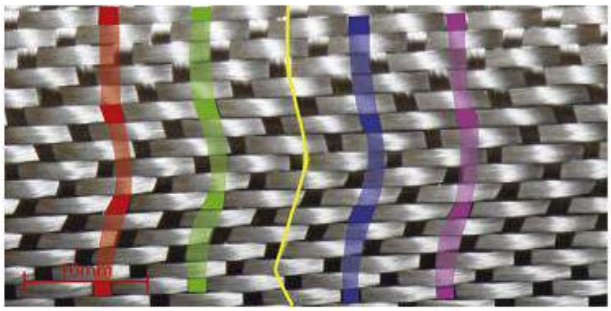

Figure 2.3: Example of misalignment in consolidation of a curved mold (Lightfoot et al., 2013a).

2.4 Characterization of dry fabrics

In practice, most of manufacturers are still facing high part failure rates due to the presence of voids, in plane fiber waviness, wrinkles and other defects during manufacturing of fabric composites (Yin et al., 2014). In particular, the complexity of forming fabrics into double curved molds through processes such as press forming has dragged researchers' attention to further characterize dry woven fabrics under fundamental deformation modes (Abdiwi et al., 2013; Yin et al., 2014). The characterization can be done in macro, meso, and micro levels. Some researchers have also employed numerical modeling tools to characterize the fabric deformation at these material levels (Boisse et al., 1997; Kawabata et al., 1973a, 1973b; Kawabata et al., 1973). A 3-D finite element model of fabrics under biaxial-tension was introduced by Gasser and his peers (Gasser et al., 2000). The model was developed with the end goal of creating more in-depth knowledge towards local deformation of yarns of fabric. Among experimental characterization works, individual tests have been performed to characterize fabrics at micro and macro levels and to assess the homogeneity of yarns (Chen et al., 2001; Peng & Cao, 2002). Between 2003 to 2005, two critical researches were reported on macro level characterization of fabrics (Peng & Cao, 2005; Peng, & Cao, 2003). In the latter work, a constitutive model was developed for fabric sheets and its parameters were found by fitting the model to bias-extension and biaxial tension tests. The most common testing modes of dry woven composites are uniaxial

tension, biaxial tension, bias extension, and picture frame shear, which are considered macro-scale characterization to understand the material's effective mechanical properties. Simultaneous tension–shear testing of fabrics was performed in 2007 by (Cavallaro et al., 2007). The author Flores-Johnson and his co workers also performed experiments to compare with simulation data (Flores-Johnson et al., 2014).

A main goal during 2D and 3D characterization of composite materials is understanding the underlying part geometrical effects (Cao et al., 2008). This is to perform forming without defects such as wrinkles or fiber breakage, the effect of processing parameters (e. g., cure time), final fiber distribution and orientation in the part (Cao et al., 2008). Scientists have specifically worked with the reinforcement fabrics and found that by controlling the fiber orientation, defects such as fiber misalignment and wrinkling can be decreased (Gereke et al., 2013). During the forming of woven fabrics, shear stiffness loss at high temperatures is also a very common problem (Spivak, 1966; Spivak & Treloar, 1967). Namely, it was found in one of the past research work of Spivak & Treloar that the mechanical shear resistance declined when Nylon monofil fabrics were set under temperature (Spivak & Treloar, 1967). Besides, it has been observed that for the sake of optimum manufacturing of structural composite parts, understanding the in-plane shear behavior of woven fabrics is critical(Colman et al., 2014). In fact, the intra ply shear is the dominant deformation mode during draping of woven fabrics, and accordingly characterization set-ups such as bias extension and picture frame tests have been widely used to understand shear stiffness of woven fabrics. Normally, in woven fabrics, the weft and warp yarns have a 90^0 relative angle at initial configuration but during draping over a double curved surface the angle between the adjacent yarns decreases (Gereke et al., 2013).

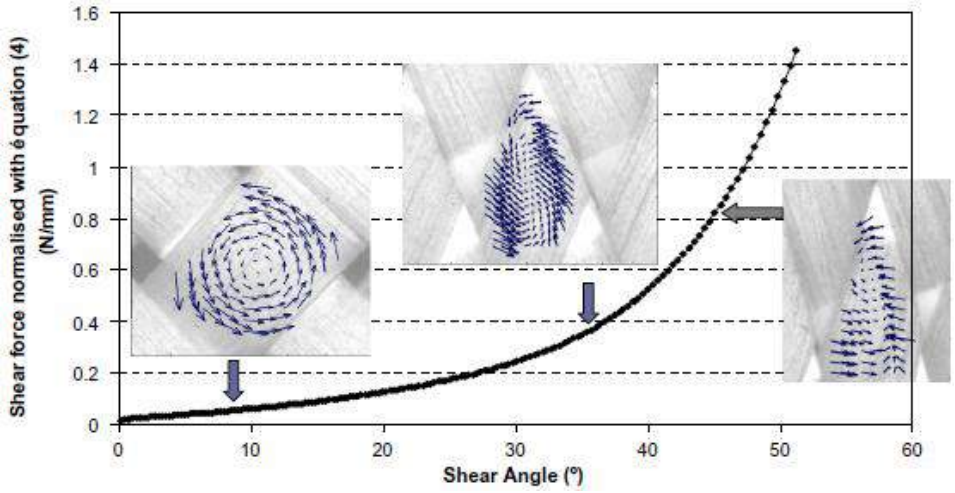

Figure 2.4: In plane shear curve of a plain weave fabric (Launay et al., 2008).

Figure 2.4 shows the in plane shear behavior of a typical plain weave where with yarns rotation/trellising shearing happens and the associated force is partly the friction occurring across the contact areas between warp and weft yarns (Gereke et al., 2013; Launay et al., 2008). With increasing shear angle to higher levels, the neighboring yarns are compressed into each other (side contact) and cause a sharp change in the material global stiffness. According to (Gereke et al., 2013; Launay et al., 2008) this critical locking angle may also be the wrinkling start.

As suggested by the current literature, a standard shear testing process for fabrics is still missing (Hamila & Boisse, 2008; Launay et al., 2008; Milani et al., 2007). Three types of shear test methods, namely the Direct Shear Force Measurement (DSFM) method, the Bias-Extension (BE) test method, and the Picture Frame test method are presently most common to observe a fabric's shear behavior and locking (Taha et al., 2013). Figure 2.5 shows a schematic of these three different shear tests. According to (Taha et al., 2013), the direct shear force measurement is a

complex process to analyze the fabric shear force as there may be a possibility of overlapping of tensile and shear stresses throughout the material.

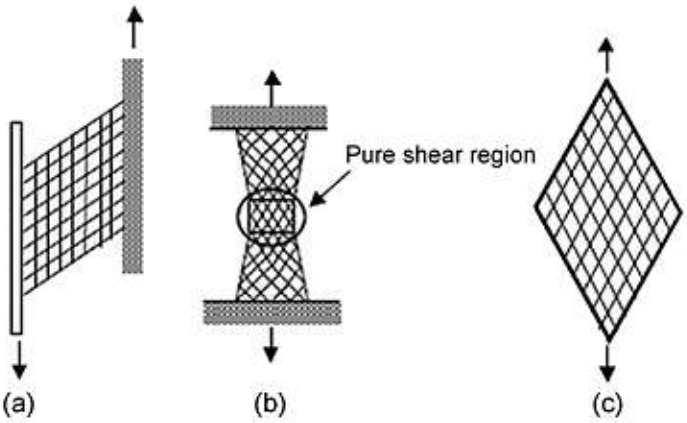

Figure 2.5: Different methods for measuring the shear properties of textiles: (a) direct shear force method, (b) bias-extension test method, and (c) picture frame test method (Taha et al., 2013).

Conversely, a simple fabric cut with ±45^{o} reinforcement angles and applying uniaxial tension makes the bias extension test method a very simple shear characterization method. However, sample slippage and fiber sliding during bias extension test is among disadvantages of this method (Taha et al., 2013). Figure 2.6 shows a typical response of the fabric under bias extension test , with sliding occurring in this case at around 60 mm displacement (Taha et al., 2013).

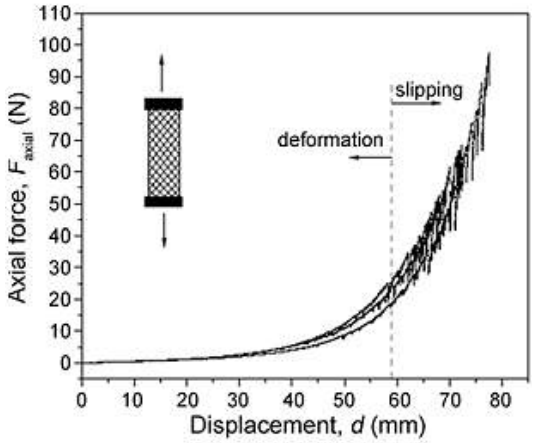

Figure 2.6: Force displacement curve from a typical bias extension test (Taha et al., 2013).

Picture frame test is more advantageous and reliable over the other two methods due to a more uniform shear force induction throughout the fabric sample. However, this test method also suffers from serve effect of misalignment (normally in the range of 1^0 to 5^0) and deviating from a pure shear mode (Milani et al., 2007). Similar to the bias-extension test , at the beginning of picture frame deformation a small force is needed for fiber yarns rotation and placement, followed by a rapid increase in the force magnitude when adjacent warp and weft yarns become packed into each other (Figure 2.7) (Taha et al., 2013).

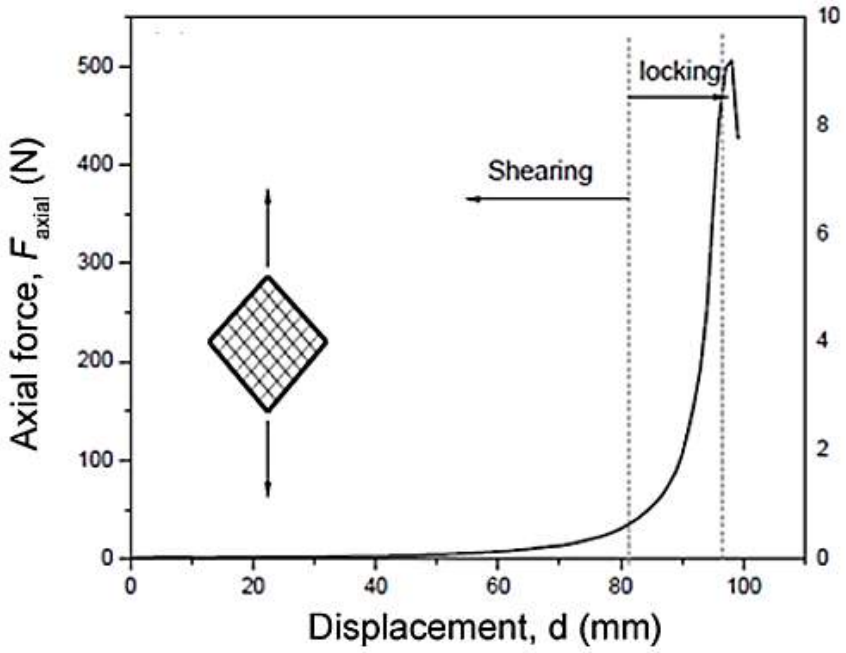

Figure 2.7: Force-displacement curve from a picture frame test showing locking and shearing regions (Taha et al., 2013).

At beginning, warp and weft yarns relatively rotates and shear force becomes very small due to friction but at high displacement warp and weft yarn become pack to each other which result sharp increase in force and obtain shear locking (Figure 2.7) (Taha et al., 2013).

Harrison (2012) compared the reliability of picture frame , uniaxial bias extension and a new biaxial bias-extension test, in order to closely observe fabric deformation and wrinkling using backlit imaging (Harrison, 2012) and found that the biaxial bias-extension testing is an accurate method of characterizing woven fabrics in combined loading modes (Harrison, 2012). Harrison also proposed that to observe deformation and associated defects in woven composites, marking tracer lines on the sample before testing and the transmitted backlit imaging can be useful. The observation of Harrison's test found that excessive loads can result in more wrinkling on the woven fabric. Normalization of characterization tests has also been a challenge to researchers in the field to generalize the characterization results (Komeili & Milani, 2013). By using iterative finite element simulations and normalization of bias extension test data, it has been observed that shear–tension tests can somewhat identify actual deformation in the woven fabrics (Abdiwi et al., 2013).

Tensile behavior of fabrics is also an important material characteristics, which can be characterized by uniaxial and biaxial tension tests (Gereke et al., 2013). A recent work presented a 3D finite element model of the tensile test for woven fabrics where experimental results were compared with the simulation model to attain specific information on ballistic application of aramid plain woven fabrics (Flores-Johnson et al., 2014).

As another type of characterization method, bending rigidity of fabrics has been tested and shown a weaker response compared to the tensile rigidity due to the relative motion of yarns (Bilisik & Yolacan, 2012; Gereke et al., 2013). The Kawabata bending test (Gereke et al., 2013; Kawabata & Niwa, 1989) and the cantilever bending test (Bilisik & Yolacan, 2012; De Bilbaoet

al., 2010; Gereke et al., 2013; Peirce, 1937) are among two most common bending rigidity test methods. Khoshbakht and peers also tested combined tension-bending behaviour of GFRP plain woven composites and found that maximum bending deformation occurred near to the fixture clamping area (Khoshbakht et al., 2009). They also performed simulations and found similarities between experimental and numerical results.

As stated before, woven fabrics are commonly used in marine, automotive, aerospace, transportation and naval architecture applications; hence they should have a high impact resistance next to their high static properties. The life time of these applications often depends on the impact life of the underlying material. It is common in practice to use nondestructive or destructive detection methods to investigate impact resistance of fiber reinforced composites. Some of the impact characterization processes in the literature have used simple visual methods (Ardakani et al., 2008; da Silva Junior et al., 2004; Nunes et al. , 2004; Shyr & Pan, 2003), and some used X ray imaging (De Morais et al., 2005; Luo et al., 2001), ultrasonic C-scanning (Aymerich & Meili, 2000) and thermal or electrical based methods (Krstulovic-Opara et al., 2011; Meola & Carlomagno, 2010).

As another characterization tool, digital image correlation (DIC) has been used by researchers to measure strain, damage modes, and in general to characterize the mechanical properties of woven fabrics (Ullah et al., 2012; Willems et al., 2008). The deformability of woven fabrics can also be tested under aforementioned characterization tests such as biaxial tension and shear tests via DIC (Willems et al., 2008). Although this imaging-based method comes from the original developments in 1980's, it has been developed over years for material testing purposes (Willems

et al., 2008) and today is frequently employed in tensile tests, flexural tests, shear tests and compressive tests, among many others (Ullah et al., 2012).

2.5 Combined loading modes

The literature shows that researchers more recently have performed numerical and experimental studies to understand the effect of fabric tension on the shear response of fabrics. These attempts were due to the high interest to know the fabric's response under combined shear–tension loading modes that are very likely in practice (both during manufacturing and service). Launay and his co-workers clearly observed the effect of tension on in-plane shear behavior of fabrics by replacing load sensors on four sides of the shear frame fixture (Launay et al., 2008). They found that shear force is higher when applying tension on the fabric. Similarly, Willems and his coworkers experimentally applied pre-tension on a fabric using a biaxial-tension fixture while applying shear (Willems et al., 2008). Other researchers (Abdiwi et al., 2013; Harrison, 2012; Harrison et al., 2012) employed biaxial bias-extension tests to induce shear tension coupling in fabrics. From the numerical studies (Harrison, 2012; Lee et al., 2009; Lee et al., 2010) it has been noticed there are fuzzy deformation regions in such combined loading modes and hence their analysis becomes fairly complex.

Over the past few years, through earlier works of (Cavallaroet al., 2004; Cavallaro et al., 2007), a new fixture was designed and manufactured via a collaboration between the UBC's Composites & Optimization Lab, the Naval Undersea Warfare Center (NUWC) and the City College of New York (CCNY) (Elliot et al., 2012). The instrument is fully capable of applying simultaneous shear tension as well as shear-compression coupling and individual uniaxial tension, uniaxial compression, picture frame shear, rotational shear and biaxial tension, biaxial

compression. This set-up has been further enhanced and used in this thesis; details will be followed in Chapter 3. Nosrat-Nezami et al. (2014) recently reported a similar shear-tension test fixture and performed characterization of coupling effect in carbon woven prepregs (Nosrat-Nezami et al., 2014). An ultimate aim of using such advanced fixtures is to enhance our understanding of mechanical behavior of composite fabrics under multitude of combined deformation modes that could not be realized via earlier test methods.

2.6 Summary

Woven and non-crimp fabrics have found a large interest in manufacturing applications in various sectors. Despite this widespread interest, there is a lack of standard methods to characterize and analyze their mechanical properties under different loading modes and to predict the formation of associated defects such as wrinkling during forming. In particular, the individual deformation modes such as uniaxial tension, picture frame shear and bias-extension have been widely studied in the past, whereas there is little information on the complexity of fabrics behavior under simultaneous/combined tension-shear modes. Moreover, there exists a gap in understanding of inter-yarn fiber sliding effect during composites processing (Mesogitis et al., 2014). To overcome this forming defect, rotational shear deformation mode of fabrics, next to the convectional trellising shear mode, should be clearly understood. In addition there is limited information in the past research on the shear-tension coupling effect in sequential combined loading modes, as opposed to simultaneous modes. These gaps led to the objectives of this thesis as listed earlier in Section 1.3.

Chapter 3: Materials and Methods

3.1 Overview

This chapter covers the experimental and statistical methods employed in this thesis. These include the biaxial-shear test set-up along with the test sample type, sample preparation, and types of deformation modes considered. Also, Digital Image Correlation (DIC) which has been one of the important experimental tools for wrinkling detection per the review is explained near the end of the chapter. The chapter is concluded with describing a statistical analysis framework for hypothesis testing between and within different deformation modes.

3.2 Experimental set-up

The main aim of using the biaxial-shear testing fixture (Figure 1.1) in this work was to run biaxial tension loading on fabrics while sequentially or simultaneously applying different shear modes (shear/picture frame and/or circular/sliding shear); the fixture will be frequently referred to as CRN instrument in the subsequent sections. The instrument is controlled via motors, load cells, data acquisition systems, which are all connected to the LabView software.

For measuring the applied load in the biaxial directions, two load cells are installed between the jaw and the lead screw plate, which can measure in-line force in each direction applied to the fabric by one motor pair. A steel coupling (Figure 3.1) is used to connect the lead screw to the rotor of the motor. The lead screw is attached to every motor pair to convert the corresponding rotational motion to a linear motion. A set screw is used in the coupling to hold the lead screw and the rotor in position rigidly. It was ensured to check the tightness of every set screw before testing a specimen. To apply shear for picture frame direction, a smaller synchronous motor was installed, which applies the load at one corner of the picture frame (Figure 3.2), up to the

maximum of ~1000N. In order to measure the load during the rotational shear mode, another DC motor has been installed as shown in Figure 3.3.

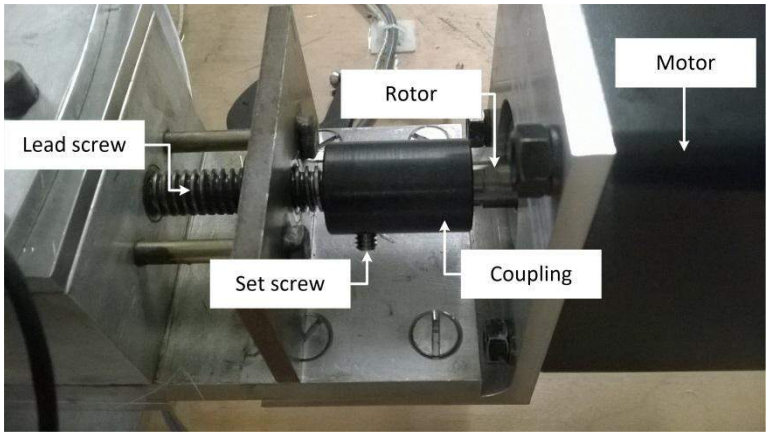

Figure 3.1: Coupling and set screw with the rotor.

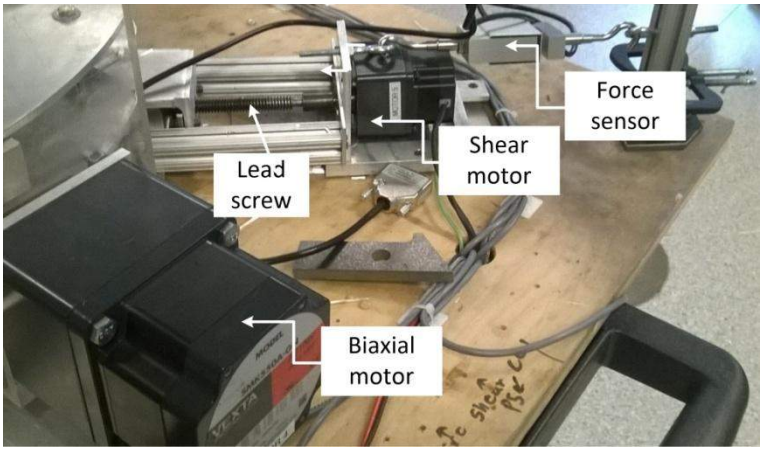

Figure 3.2: Shear motor and force sensor.

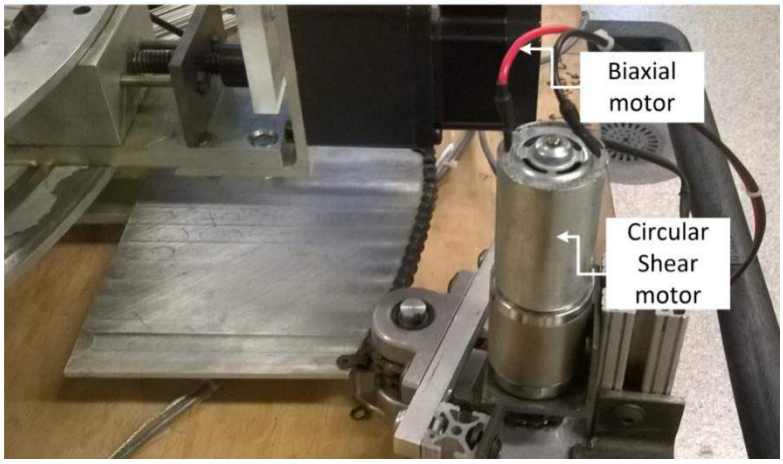

Figure 3.3: Circular shear motor.

The biaxial-shear tester was operated using a NI LabView program (version 2011). The biaxial load cells are capable to measure a maximum 2500 N of force in each axis direction. During each test, a maximum force value had to be set in the LabView front panel. The experiment can then be automatically stopped by the load cell by presetting this maximum value. For displacement measurement in biaxial and shear directions, high resolution linear variable differential transducers (LVDTs) were used (Figure 3.4). In the biaxial direction, the LVDT provides axial displacement and in the picture frame direction the LVDT provides shear displacement. It should be noted that as the individual motors in the two motor pairs are similar, for measuring net displacement in one direction, the LVDT measurement should be multiplied by two. Similarly, to measure the shear displacement in the picture frame mode, the corner of the frame movement was observed by the LVDT. Finally, the test data were collected using National Instrument data acquisition module and LabView. Since, the shear displacement is generally larger than the biaxial direction displacement (a fabric is much stronger in tension than in shear), a large stroke range ($\pm 1.27\ \mathrm{cm}$) was used to measure the shear displacement. For the biaxial direction, a shorter stroke range ($\pm 0.635 \mathrm{cm}$) was used to avoid rapid fiber failure.

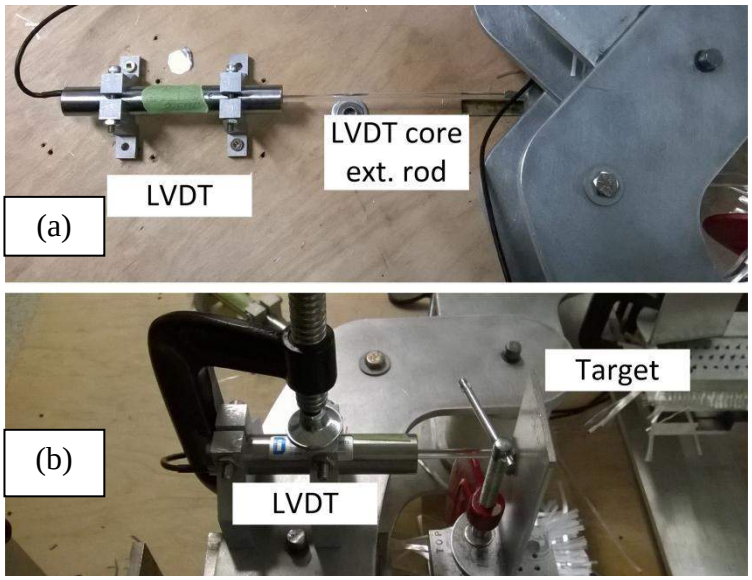

Figure 3.4: (a) LVDT for Shear displacement measurement, (b) LVDT for axial displacement measurement.

As fiber slippage is one of the major difficulties in fabric testing, which often occurs between the fabric sample and clamps, a custom-designed needle clamping system along with proper mounting contact was used (Figure 3.5). This clamping system could successfully eliminate the slippage of the test samples, while allowing the yarns to freely rotate along needles under shear modes; for more details please also see (Nosrat-Nezami et al., 2014).

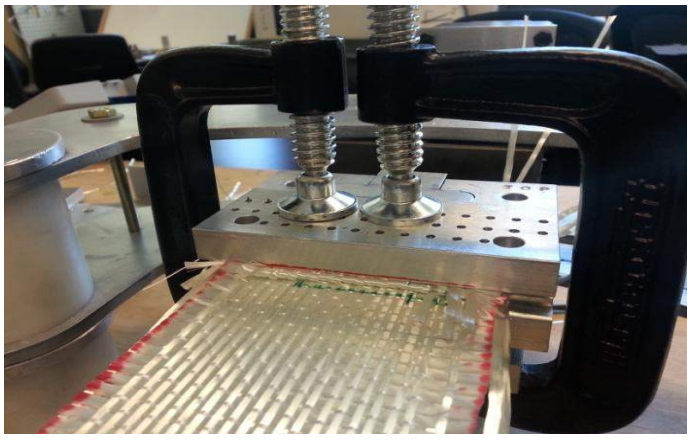

Figure 3.5: Fabric clamping with needle jaw and C clamps to ensure proper contact.

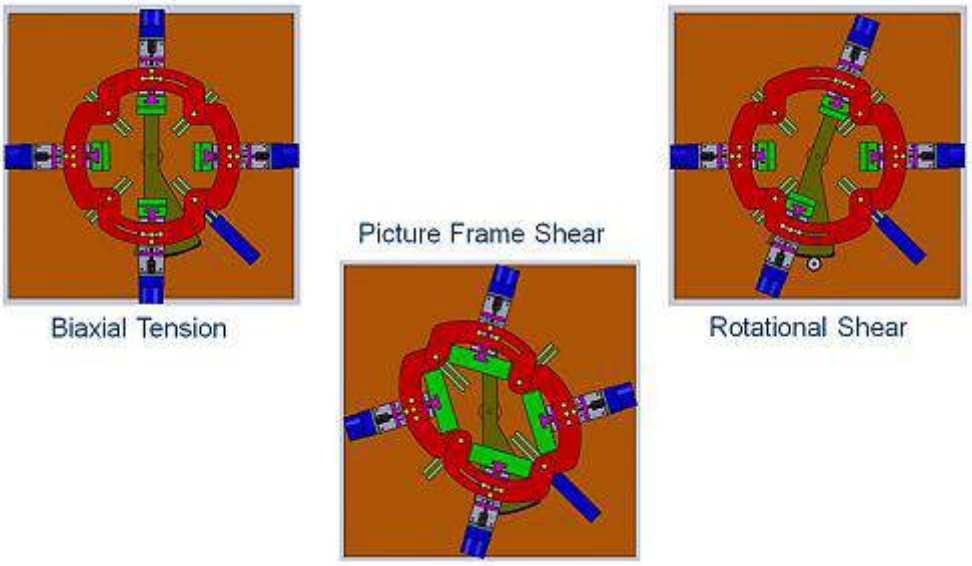

Figure 3.6: The induced deformation modes by the test fixture (Elliot et al., 2012).

3.3 Types of tests with biaxial-shear fixture

Figure 3.6 schematically shows three fundamental deformation mechanisms induced by the biaxial-shear test machine. The combined loading modes can accommodate any combination of the above three modes. In total, the instrument may be run in seven deformation modes which are discussed in the following sub-sections. Figure 3.7 shows the final assembled set-up used in this work.

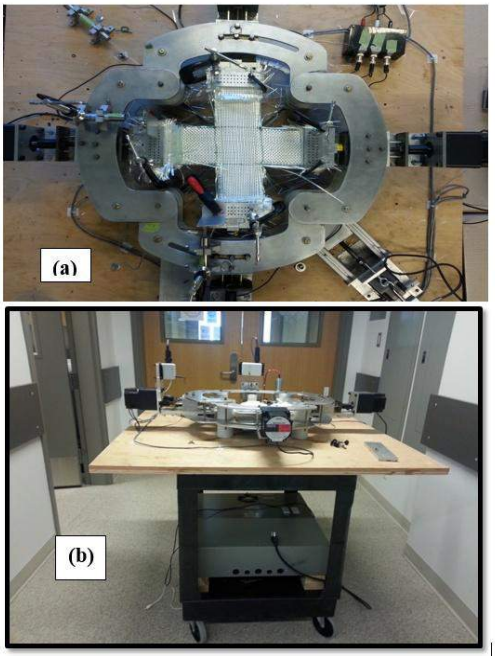

Figure 3.7: The biaxial-shear test set-up; (a) top view, and (b) side view.

3.3.1 Pure biaxial tension mode

A schematic of deformation in this mode is shown in Figure 3.8. Decrimping of warp and weft tows when extended concurrently prompts non-linearities in the mechanical response of the fabrics (Boisse et al., 2011). More specifically, as a result of the inter-locked architecture, the tensioning/decrimping in the warp and weft yarns become inter-dependent and yield complex meso-level deformations. Biaxial properties of several fabrics have been tested in the past research work (Buet-Gautier & Boisse, 2001; Carvelli et al., 2008; Kawabata et al., 1973; Willems et al., 2008). Relating to the same efforts, the present research used the pure biaxial mode with the CRN instrument using a Fiberglass fabric (more details of the material will be presented in Section 3.4).

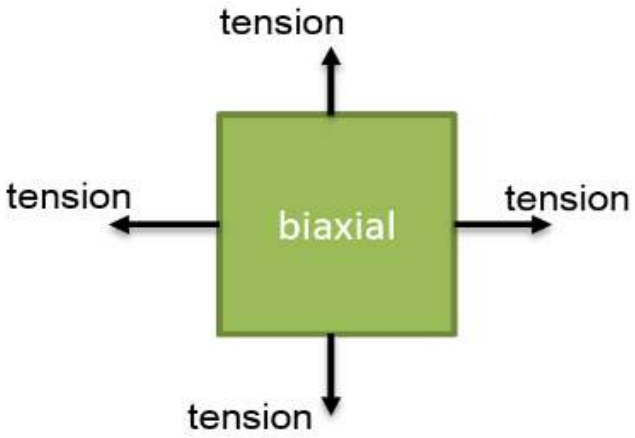

Figure 3.8: Schematic of a pure biaxial mode.

3.3.2 Pure shear (picture frame) mode

The schematic of pure shear (picture frame/PF) mode is shown in Figure 3.9. Although the previous literature showed that up to ~50^0 shear deformation is possible for some fabrics (Cao et al., 2008), the set-up used in this work allowed to reach a maximum of 15^0 picture fame shear. Theoretically, the initial square (blue) region of a fabric cell (Figure 3.9 (a)) is changed to a rhomboid shape after pure PF shear (Figure 3.9 (b)).

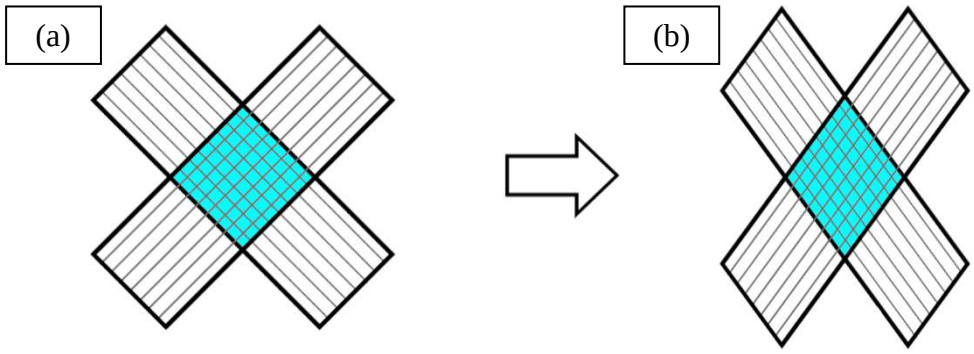

Figure 3.9: Schematic of pure shear mode showing shear deformation without yarn slippage; (a) initial region before PF shear , (b) deformed region after PF shear .

3.3.3 Pure circular shear

Per (Komeili, 2014), it is critical to recognize a fabric's shear behavior with and without yarn rotation. Ordinarily, a change in angle between adjacent warp and weft yarns is referred to as shear in fabrics. However, shear angle can likewise happen with rotation of yarns instead of trellising similar to Figure 3.10 (b). The CRN set-up provides both "picture frame" or "pure shear" and "circular (rotational)" shear testing possibilities. The circular shear mode is a rather new mode of shear deformation considered in the recent literature of fabrics due to its application in structures such inflatable tubes (Cavallaro et al., 2003). The fundamental difference between this shear mode and the PF mode is that in the rotational/circular mode the yarns and crossover points do not remain at the same point after deformation (Komeili, 2014), as shown in Figure 3.10. The schematics used for PF and circular/rotational shear modes in the subsequent graphs of the thesis are shown in Figure 3.11.

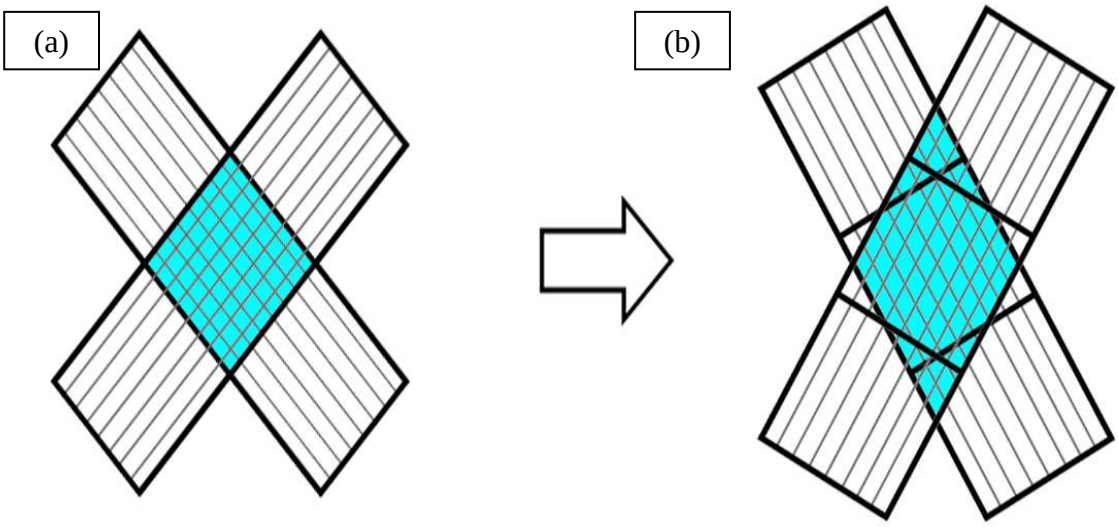

Figure 3.10: The schematic of rotational/sliding shear; (a) initial region before CS shear, (b) deformed region after CS shear.

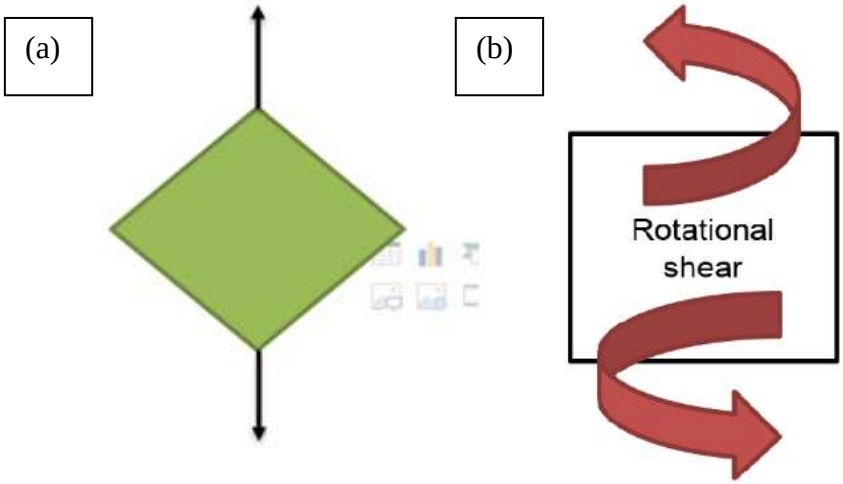

Figure 3.11: The basic fundamental difference of loading applied in the picture frame and rotational shear modes; (a) picture frame shear, (b) rotational shear.

3.3.4 Simultaneous biaxial tension and PF shear

The CRN set-up can perform characterization of dry fabrics when the biaxial tension and picture frame shear motors working at the same time. Schematically shown in Figure 3.12, this combined deformation mode has also found in recent literature (Cao et al., 2008; Nosrat-Nezami et al., 2014).

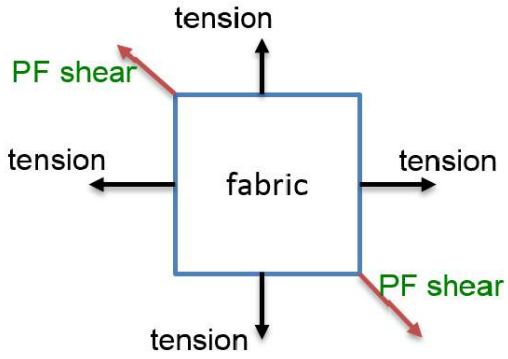

Figure 3.12: Schematic of Simultaneous biaxial +PF deformation mode.

3.3.5 Simultaneous biaxial tension, PF shear and circular shear

The CRN set-up has been designed to characterize fabrics behavior under combined biaxial, PF shear and circular shear modes. Figure 3.13 shows the schematic of this mode, which causes a

severe deformation and coupling behavior in the fabric as will be shown in Chapter 4. No earlier work has addressed this mode in literature.

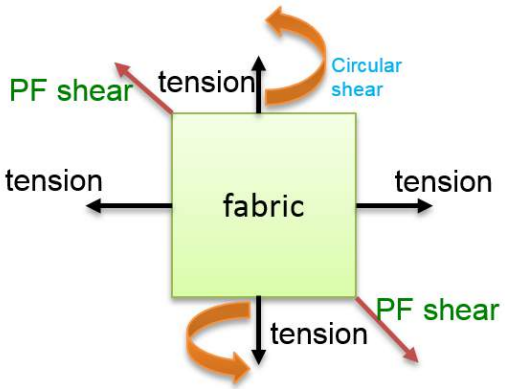

Figure 3.13: Schematic of simultaneous biaxial +PF +circular shear deformation mode.

3.3.6 Biaxial tension affected shear (a sequential coupling effect)

Fabrics can experience PF shearing after going through a pre-biaxial tension under this deformation mode. The CRN set-up was used to perform this coupling test where at first 1000N biaxial force was applied to the fabric, and afterward the picture frame PF shear was applied up to 15 degrees. Figure 3.14 shows the schematic of the biaxial affected shear deformation mode where the numbers 1 and 2 points to the sequence of applied loads.

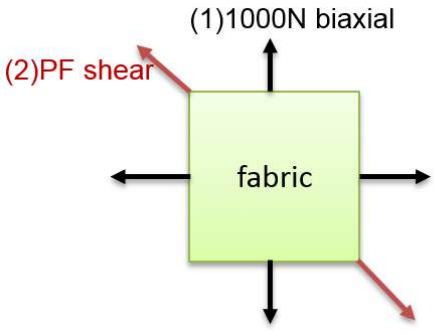

Figure 3.14: Schematic of biaxial affected shear deformation mode.

3.3.7 Shear affected biaxial tension (a sequential coupling effect)

In contrast to Section 3.3.6, in this coupling mode the fabric firstly observes 15^0 picture frame shear as marked by number '1' in Figure 3.15 and afterwards that biaxial tension is applied to the fabric, which is marked as '2' in the Figure.

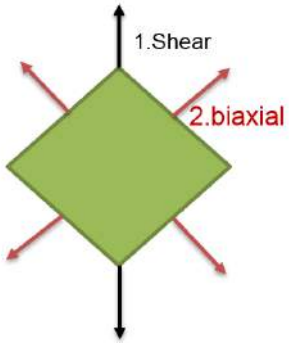

Figure 3.15: Schematic of shear affected biaxial deformation mode.

3.4 Test material

A heavy triaxial [0, 90, 0] dry Fiberglass non-crimp fabric was provided by Campion Marine Inc. and used in this research. Table 3.1 presents the summary of the material specifications and Figure 3.16shows an image of the fabric. Per convention, the fabric roll direction was used to determine the warp direction (Figure 3.17).

Table 3.1: Description of the fabric material used in this research (adapted from TDS -Texonic JB Martin).

Commercial code	**E-Glass TG-54-N**
Nominal weight (g/m^2)	1824
Standard roll length (m)	35
Resin compatibility	Polyester, Venylester, Epoxy
Compressed thickness (mm)	1.52
Wet layup thickness (mm)	2
Warp fill ratio (%)	52
Warp end counts (per cm)	8
Weft end counts (per cm)	11.4

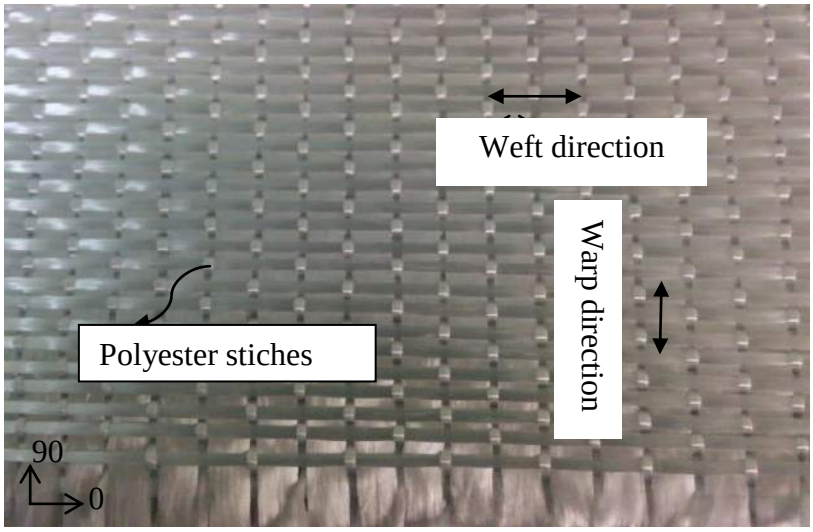

Figure 3.16: E-Glass TG-54-N Fiberglass fabric sample used in the experiments.

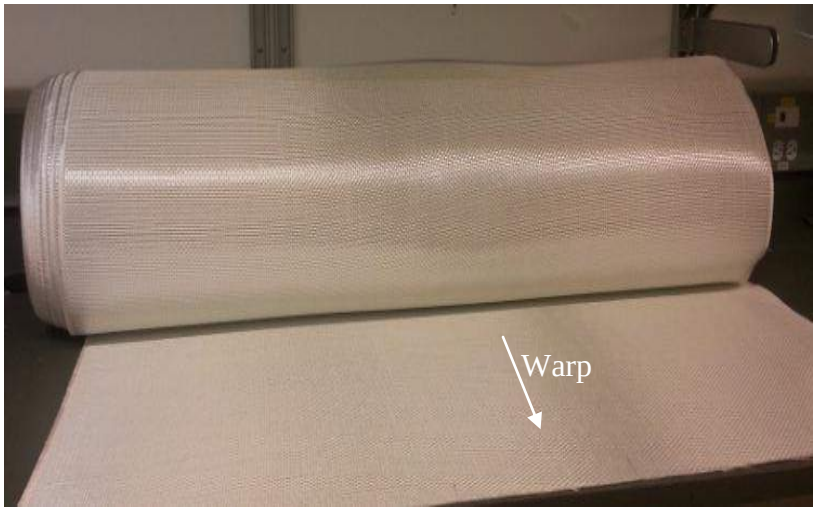

Figure 3.17: Fiberglass fabric roll manufactured by Texonic JB Martin.

3.5 Other experimental considerations

3.5.1 Sample preparation and mounting

The cross-shape samples used in the CRN set-up is shown in Figure 3.18, each strip of the cross having 450 mm length and 100 mm width. It is to note that long and narrow shape samples are generally found better for uniformity of deformation in the middle zone of interest, when compared to square cut samples (Spivak & Treloar, 1967). As addressed in Section 3.2, the CRN test set-up uses needle clamps (Figure 3.19(a)) to perform tests, for which the above mentioned test sample size was long enough. The reason of longer sample was that the edge of the sample was folded (thought it is optional) with the needle of the jaws to further avoid fiber slippage.

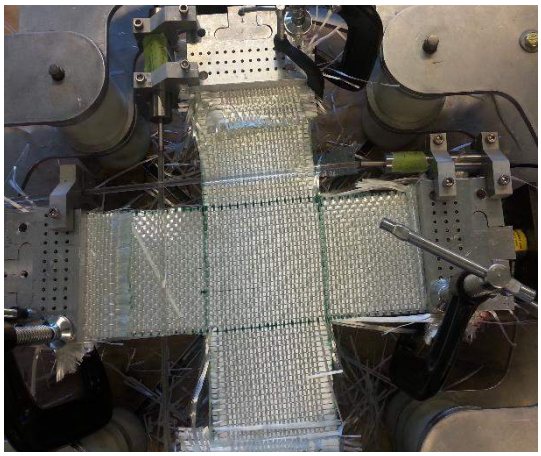

Figure 3.18: Fiberglass test sample shape used for biaxial, pure shear, and combined deformation modes.

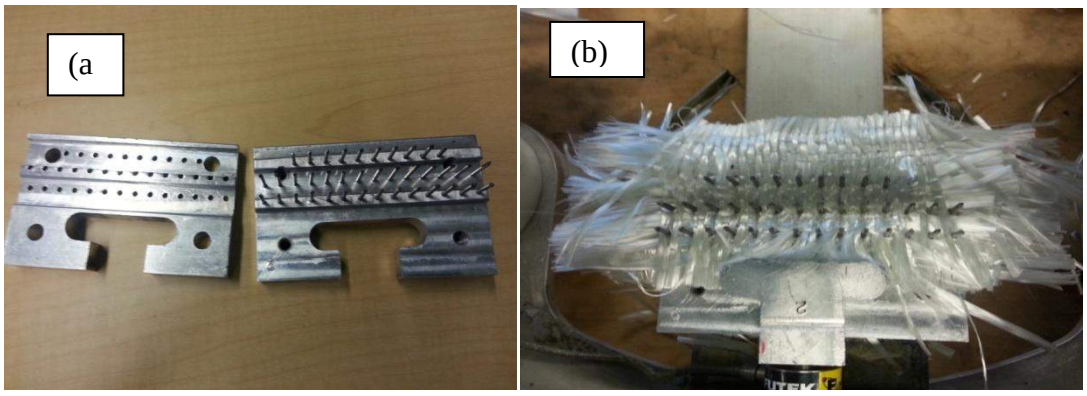

Figure 3.19: (a) Needle clamps used for mounting samples (b) Extra scarp layers of fabric in needle clamp that further helped obtaining a slippage-free mounting.

In addition, two scarp layers of fabric pieces could also be inserted (Figure 3.19 (b)) to further increase the friction in the clamp area and allow reaching the maximum load of the machine during tensile testing while removing any fiber pull-out in the clamp area.

3.5.2 Uniaxial validation test

To ensure the reliability of the CRN set-up measurements, first it was compared with a standard Instron machine under uniaxial tensile mode. For each test, in warp or weft direction, using the Instron and biaxial-shear CRN machines (Figure 3.20), three repeats were conducted. By choosing rubber furrowed surfaces square to clamp the fabric sample, Instron machine offered a standard clamping of fabric test materials. This rubber maid clamp has also been utilized in

custom created fixtures by other researchers (Willems et al., 2008). A procedure similar to ASTM D5035-11 was followed for the Instron test. Namely, the textile sample was cut into 160 mm gauge length, which was the distance between two grips, and 60 mm wide where 18 yarns in the sample existed. The speed of the test was 6mm/min and a slight pre-tension was applied before the actual test to straighten the fabric. The sample width of the CRN uniaxial test was nearly the same as before, but the gauge length was 180 mm given the jaw-to-jaw distance of the set-up. The results of this validation test will be presented in the next chapter.

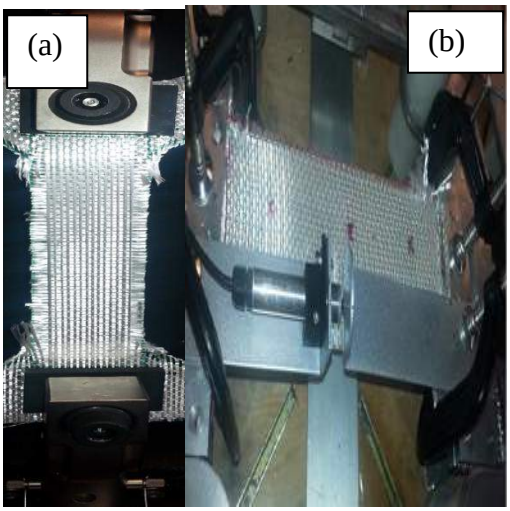

Figure 3.20: Fixure used for uniaxial testing with (a) Instron set-up, and (b) CRN set-up.

3.5.3 Force normalization and limitation

While for axial modes the force normalization is straightforward (dividing the force by the number of yarns in the loading direction or sample width; e. g. (Launay et al., 2008), according to (Cao et al., 2008; Komeili & Milani, 2013) the picture frame shear force normalization is slightly more intricate. Namely, the shear angle ɣ and shear force Fsh should be first calculated based on the frame kinematics by Equations (3-1) to (3-3). The PF shear test data can then be normalized by Equation (3-4).

$$\gamma = 90° - \Theta \tag{3-1}$$

$$\mathrm{Cos}\Theta = \frac{\sqrt{2}\mathrm{Lframe} + \mathrm{d}sh}{2\mathrm{Lframe}} \tag{3-2}$$

$$\mathrm{Fsh} = \frac{\mathrm{F}}{2\mathrm{Cos}\Theta} \tag{3-3}$$

$$\mathrm{Fnormalized} = \mathrm{Fsh}\frac{\mathrm{Lframe}}{\mathrm{Lfabric}^2} \tag{3-4}$$

The frame length, lframe, shear displacement, d_{sh} and the length of fabric, Lfabric, as well as the frame angle Θ are shown schematically in Figure 3.21.

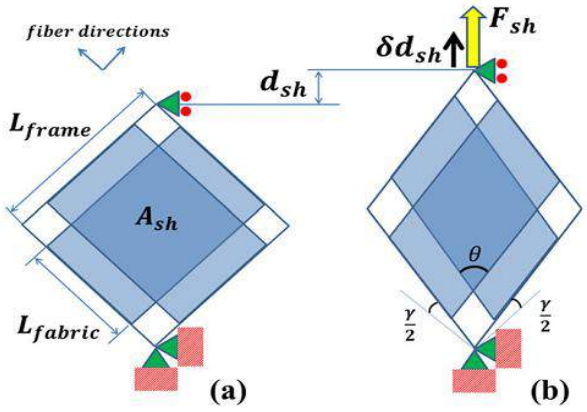

Figure 3.21: Geometrical configuration of PF test (a) before (b) after deformation (Komeili & Milani, 2013).

As mentioned earlier, another shear test that was performed by the CRN instrument was circular shear. As an example of this mode, Figure 3.22 shows the fabric's one direction rotated with the sliding direction due to the circular force. The circular shear force was measured from the load cell attached to the motor and the sliding shear angle of the yarn was measured by tracking the marks on the yarns of deformed fabric. There is no standard formula currently in the literature

for normalization of this mode, and hence the force magnitude is reported directly. Finally, there was a limitation on the set-up at the time of these experiments on full calibration of magnitudes of picture frame shear force; hence the data collected from this test were opted to be used only a qualitative manner in the results to be presented in Chapter 4.

Figure 3.22: Sliding shear experiment was performed using CRN set-up.

3.6 Digital image correlation (DIC)

DIC is a non-contact full-field strain measurement system, which allows fully mapping and tracking surface displacements in three dimensions, in the order of micro-strains. The DIC instrument can be used for measuring displacement, strain, and different geometrical options associated with the deformation of fabric specimens (Komeili, 2014). The steps needed for running DIC in the present work were as follows.

3.6.1 Preparing the samples for DIC

DIC system generates the material surface by estimating the position of unique features inside a square region called ‘facet’. The software that comes with the employed DIC system (Instra4D) generates facets as shown for a small region in Figure 3.23. The way that each facet is uniquely recognized in the software is the patterns of features inside the facet. Thus, it is ideal to have a random distribution of white and black spots inside each facet (two colors with a high contrast);

this is called a speckle pattern. Samples of speckle patterns are shown in Figure 3.23 (a) and (b) during fabric testing. It is important to note that before performing a test, an effective calibration in the DIC software is required, which means in the black-white calibration plate, green dots should form, instead of red or yellow dots. The red and yellow dots will mean a poor and an average quality of the speckle pattern, respectively.

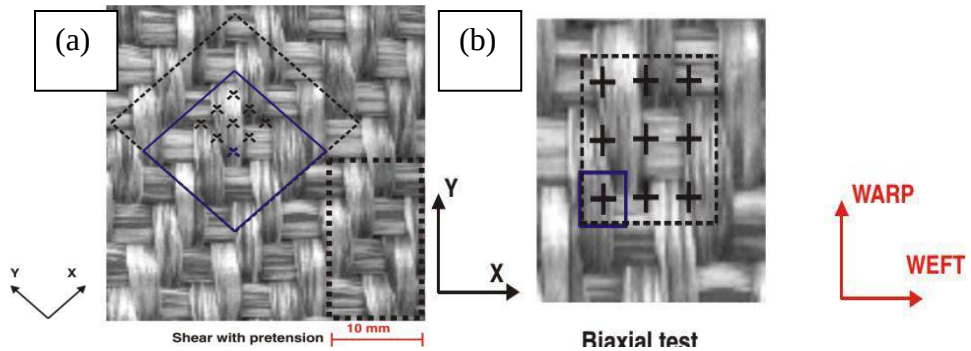

Figure 3.23: DIC steps after calibration of a speckle pattern,(a) example of strain window with speckle pattern in the fabric during shear test with pre-tension and (b) during a biaxial test (Willems et al., 2008).

In order to make a speckle pattern on a given material surface, different methods may be used, including a spray can, use of a toothbrush and ink, or simply printing of speckle pattern. Here, in order to make speckle pattern, the toothbrush and spray methods were considered. The two methods were first practiced individually and finally a combination of them (spraying on brush and splitting the brush on the dry fabric) gave the most successful result to get a correct speckle pattern. It provided 100 % green marked calibration.

3.6.2 Preparing the test set-up

One of the important cares to be taken in getting accurate results from stereovision is to assure proper location of cameras. Figure 3.24 shows the placement of cameras during running a sample test. It was found that the perfect condition for a test is attained when both cameras are having the sample in their center of view and there is an angle of 40 to 60 degrees between the cameras. LED lights can be turned on to increase the light intensity, but they must be avoided in the case

of shiny surface or high reflections. If LED lights are connected to the control box they can be turned on by a switch on the back of the box.

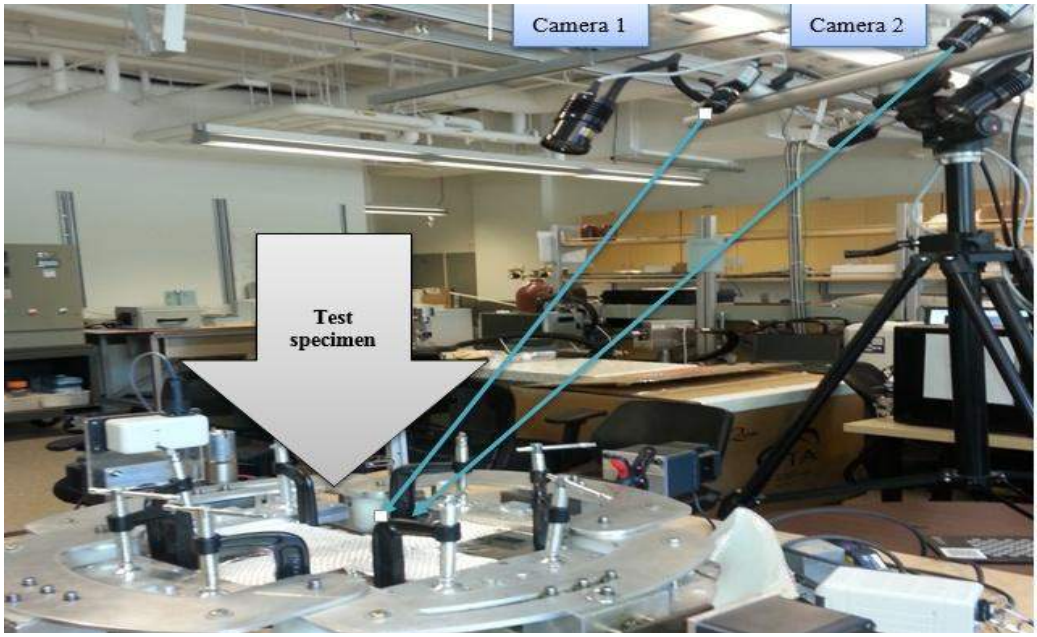

Figure 3.24: DIC cameras during a test with the biaxial-shear fixture.

3.6.3 Wrinkle detection with DIC

The sample was prepared for DIC analysis and clamped in the CRN fixture. Next, calibration was done by the calibration plate and before starting a test one image was taken as a reference image. After that the corresponding test (simultaneous shear-tension test and another time a pure PF shear test) was performed. During the test images were taken continuously. Figure 3.25 shows the example of clamping E-Glass TG-54-N fabric while PF shear testing with DIC. Any notable local z-displacement (out of plane) in the DIC images can be attributed to wrinkling.

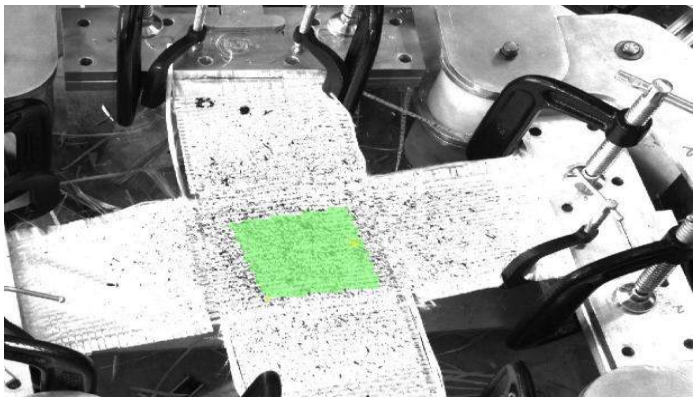

Figure 3.25: E-Glass TG-54-N fabric during wrinkle test with DIC.

3.7 ANOVA statistical analysis framework

ANOVA is one kind of statistical hypothesis testing, which has a great use in experimental data analysis (Bilisik, 2011; Işık & Ekici, 2010; Montgomery, 2008). Experimental data is often used by analysts to make decisions on the choice of a material/process/etc. based on testing associated null hypothesis (Smith & Vaidya, 2013). Rejecting a null hypothesis is statistically considered as significant when the probability P-value is less than 0.05. However the acceptance of the null hypothesis occurs when the probability P-value is higher than 0.05.

During the experiments under different deformation modes, the axial displacement and/or shear angle were applied to dry fabric at different deformation modes while the axial forces and/or shear force as well as wrinkle were observed at the output. Considering the set-up and material experimental conditions, every test configuration may have experienced some noises, such as machine vibration, sample preparation and handling errors, LVDT sensor set-up and fabric clamping, inherent fiber misalignment variation from one sample to another, etc. (Figure 3.26). Under such noise factors, statistically speaking, one should expect that the output measurements have some random variations (i. e., test non-repeatability). Hence, the significant outcomes of the

tests (e. g., effect of deformation mode, coupling effect, etc.) must be analyzed statistically; otherwise they will be more subjective.

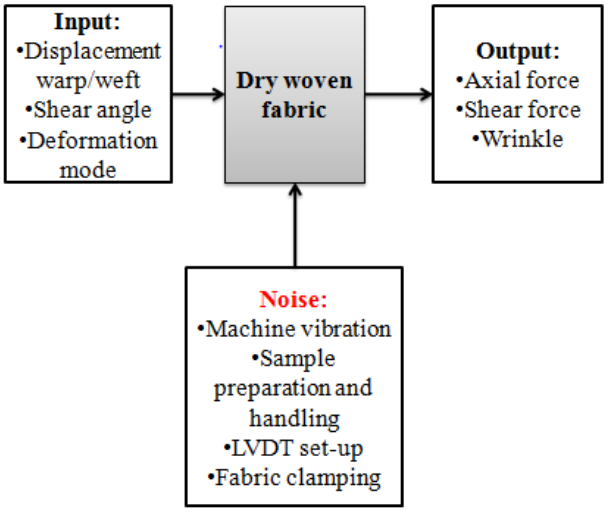

Figure 3.26: Schematic of the experimental input, output and noise to observe the importance of statistical analysis.

The experiment was performed with three replications, but due to high levels of noises only one of three experiments got the reliable data for different deformation modes. Due to the noise effect two of the three repeats observed slippage and uncertainties. So we took the one most reliable and meaningful repeat data among those three repeats with high stiffness and positive slope. However, still the effect of noise was present in that data which was needed to be accounted. In order to account for random noises during the tests and find the correct significance of test outcomes, two-factor ANOVA statistical analysis of deformation modes was considered with interaction terms representing the random error. Namely, one factor was the controlled displacement level (or shear angle in the shear mode), the other factor was the main targeted treatment (e. g., the type of deformation mode such as shear vs. simultaneous, or the effect of reinforcement direction, such weft vs. warp given a test mode) (Figure 3.27). More specifically, e. g., between the two deformation modes, at each given displacement level (or

shear angle) there are two means which are considered as μ_1 and μ_2. The test hypotheses are: H_0: $\mu_1=\mu_2$ and H_1: $\mu_1\neq\mu_2$. The means of the material response in the two deformation modes are statistically the same when the corresponding P-value is greater than 0.05 and the null hypothesis H_0 is not rejected. On the other hand, the means of the material response in the two deformation modes are different when the P value is lower than 0.05 and the null hypothesis is rejected(Montgomery, 2008). To do ANOVA analysis, the experimental data were also normalized according to the deformation types as discussed in Section 3.5.3. Table 3.2 outlines one example of ANOVA statistical analysis at two deformation modes. Here at Mode 1 and Mode 2, the effect of input displacement and the deformation mode factors on the output normalized force can be analyzed by two-way ANOVA. The targeted null hypothesis is that the force response in the two modes of deformation is statistically identical on average.

Table 3.2: Framework for ANOVA analysis in an example with two types of deformation modes as well as eight displacement levels as input factors and the force response as the output.

Mode1		**Mode2**	
Displacement	Normalized force	Displacement	Normalized force
d1	f1	D1	F1
d2	f2	D2	F2
d3	f3	D3	F3
d4	f4	D4	F4
d5	f5	D5	F5
d6	f6	D6	F6
d7	f7	D7	F7
d8	f8	D8	F8

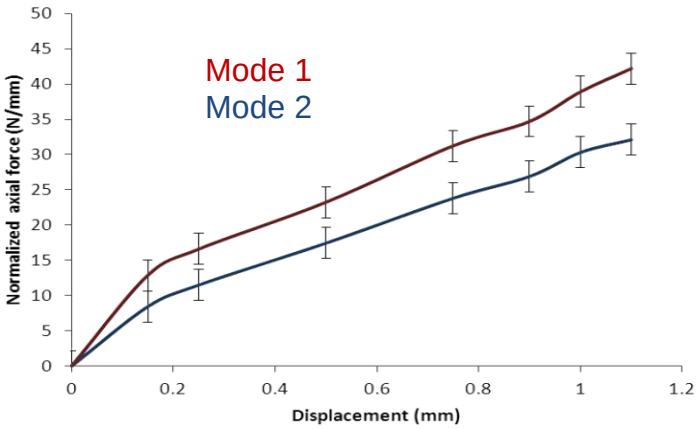

Figure 3.27: Example of force response in two different deformation modes at different controlled displacement levels; for subsequent ANOVA analysis to test whether or not the two curves are different (i. e., checking the effect of deformation mode).

3.8 Summary

An advanced experimental set-up was described for fabrics characterization under seven individual and combined deformation modes. the biaxial-shear set-up is also capable of preforming bias-extension test for shear characterization; however excessive fiber slippage is among disadvantages of the latter test method (Taha et al., 2013) and it was decided to use the picture frame mode in this research, along with a separately controlled circular/sliding shear mode. Sample preparation, clamping, and force normalization was outlined. DIC set-up was discussed and showed how to identify wrinkle and strain in a deformed fabric. With reference to earlier works, it was speculated that a non-linear behavior and high shear-tension effect should be expected in the proposed tests. To account for the effect of noise in experimental results, however, the application of two-way ANOVA was deemed critical.

Chapter 4: Results and Discussion

4.1 Overview

In this chapter, the results of different modes of experiments will be discussed. The uniaxial validation test result of the biaxial-shear CRN set-up will also be presented. Each of the test modes, including the uniaxial mode, is analyzed under a two-way ANOVA framework as discussed in the previous chapter. Moreover, the findings of digital image correlation (DIC) test will be presented in this chapter.

4.2 Validation testing

Before running the main set of experiments, it was required to test whether or not the data from the custom biaxial-shear instrument are reliable/correctly calibrated. On the ground of this reason, the result of a uniaxial testing with the CRN machine were compared with those from a standard Instron universal tensile machine as follows.

4.2.1 Uniaxial test with Instron

The uniaxial tension test was performed in both warp and weft directions of the Fiberglass fabric in an Instron machine (Figure 4.1). Warp and weft mechanical responses showed very different values (Figure 4.1), where the normalized axial force (i. e., force per yarn) was higher in the weft direction, indicating some unbalancedness in the composite material. At a displacement of around 1.2 mm, the maximum uniaxial force in the weft direction was 42.2 N/yarn, whereas in the warp direction the uniaxial force was 32.1 N/yarn (i. e., ~25% mechanical unbalancedness). However, to objectively rely on this directional difference in the material mechanical behaviour, statistical analysis was needed. Using ANOVA with two factors, the null hypothesis acceptance would mean that warp and weft direction properties are the same on average. Inversely, the null hypothesis rejection condition indicates that the warp and weft properties are different. The

ANOVA resulted in a P-value of 0.008 which means that the warp and weft yarns indeed behave differently under uniaxial extension model, for the given Fiberglass material.

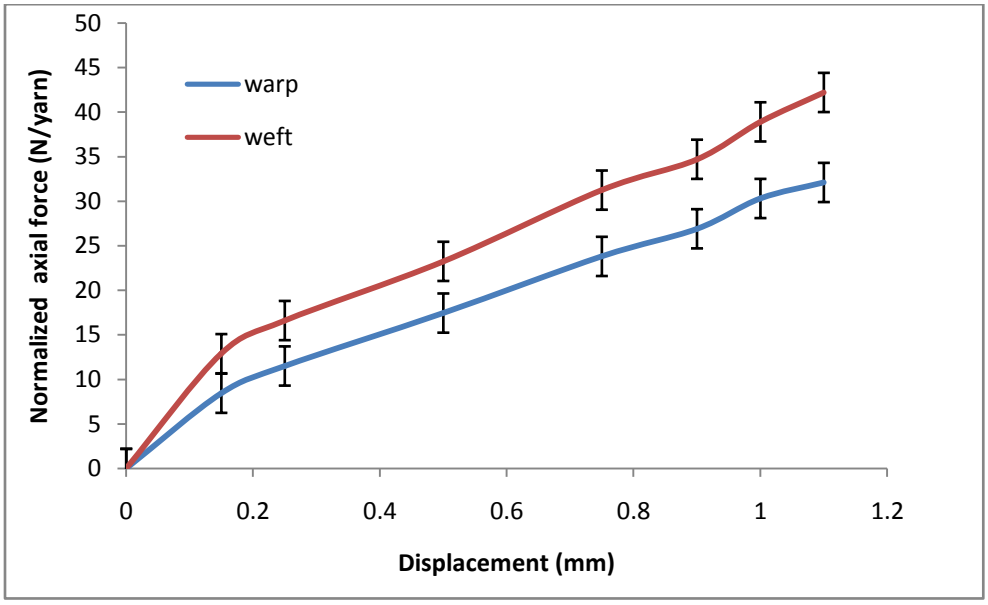

Figure 4.1: Uniaxial test on the Fiberglass fabric in the Instron machine.

4.2.2 Uniaxial test with CRN

Uniaxial tension was realized in both warp and weft directions of the material in biaxial-shear CRN machine. The displacement was measured by the LVDT sensors. Similar to the tests of Instron machine, the uniaxial force was higher for the weft yarns than the warp yarns (Figure 4.2). At 1.1 mm displacement, the maximum uniaxial force per yarn was 86.6 N/yarn in the weft direction, whereas in the warp direction it was 42 N/yarn (i. e., ~50% difference); however, as indicated by the mean error bars, the noise level in the custom set-up was higher than those in Figure 4.1.

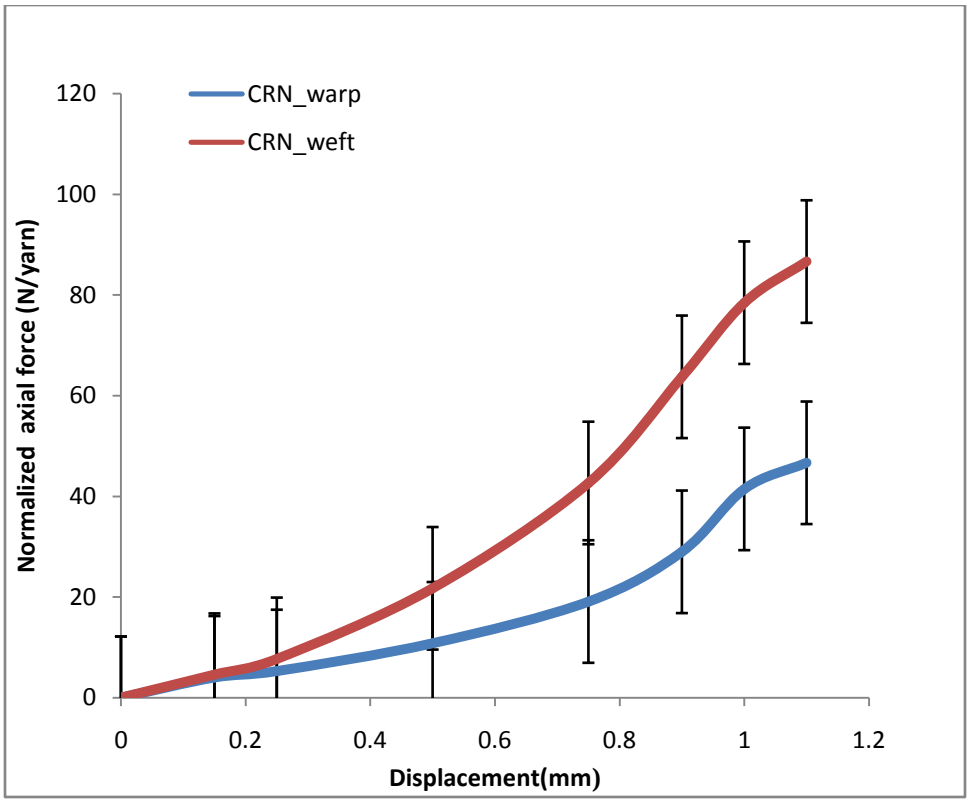

Figure 4.2: Uniaxial test on Fiberglass fabric in the biaxial-shear CRN machine.

Statistically, ANOVA analysis showed that the P value in this case is 0.004, which once again similar to the previous test, it means the null hypothesis can be rejected and the warp and weft responses for uniaxial tension mode are different from the given fabric.

4.3 Comparison between Instron and CRN set-ups

Combining the experimental date of Figures 4-1 and 4-2 within the same graph (Figure 4.3), it can be seen that in reality, uniaxial tension response of fabrics is the same for both set-up conditions, especially for the warp yarns. Similarly, the weft yarns' uniaxial response matches between the two different instruments, especially at lower extensions. The higher variation in the weft yarns response may be attributed to higher fiber count in this direction (Table 3.1 and Figure 3.16). These are, however, general qualitative conclusions and ANOVA analysis was next performed to ensure the comparison objectivity.

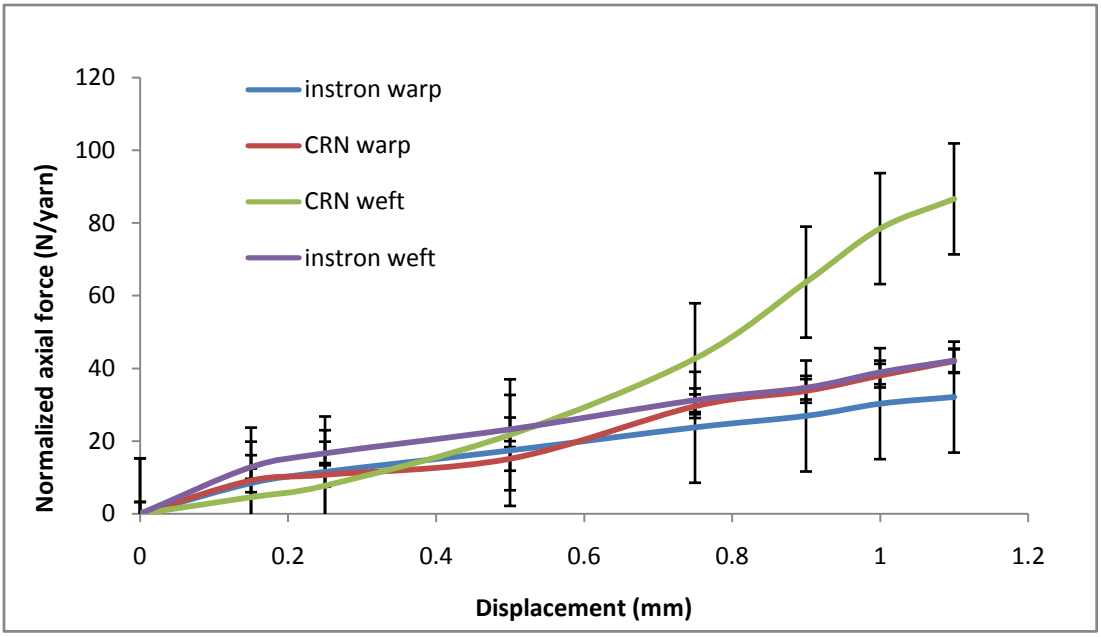

Figure 4.3: Comparing the uniaxial responses of the Fiberglass fabric in the warp and weft directions in Instron and biaxial-shear CRN machines.

The null hypothesis in the ANOVA analysis was that if the P - value>0.05, then the two machines are overall giving the same response, which means the test custom set-up is reliable to do further experimental tests. In opposite, the rejection of the null hypothesis (P<0.05= α) would inform that the set-up is not reliable as the responses are not matching. From Table 4-1 warp result, it can be seen that displacement factor shows a P- value of 6.9E-5< 0.05 or F= 35.06> 3.79= F-crit, hence the null hypothesis is rejected, meaning that as expected in both machines the higher extension shows the higher force. For the machine type factor, however, the P value is 0.068 > 0.05 or F= 4.6< 5.59 = F-crit, which explains that the null hypothesis cannot be rejected and for that reason at 95% confidence interval there is no significant difference in the output of the two machines.

Table 4.1: ANOVA results between the Instron and biaxial-shear CRN set-ups in warp and weft directions, under uniaxial tension mode.

Warp direction						
Sources of variation	SS	df	MS	F	P-value	Fcrit
Displacement level	2517.412	7	359.6303	34.05916	6.90681E-05	3.78704354
Machine type	48.68551	1	48.68551	4.609837	0.068912843	5.591447848
Error	73.92854	7	10.56122			
Total	2640.026	15				
Weft direction						
Sources of variation	SS	df	MS	F	P-value	Fcrit
Displacement level	8263.95	7	1180.564	5.062235	0.024139962	3.78704354
Machine type	699.3655	1	699.3655	2.998865	0.126930965	5.591447848
Error	1632.471	7	233.2101			
Total	10595.79	15				

Considering he weft direction results in Table 4-1, again the displacement factor shows the P-value of 0.02< 0.05 or F=5.06> 3.78= F-crit, which concludes at 95% of confidence interval the force output in both machines are varying with the displacement change. However, for the machine type factor results show the P-value of 0.13 >0.05 or F = 2.99 < 5.59 = F-crit, which suggests that the null hypothesis cannot be rejected. That means in 95% confidence interval, the force outputs coming from the two machines are the same in the weft direction.

4.4 Pure biaxial test

Pure biaxial tension was applied to the Fiberglass fabric test material. In the past, numerous research efforts (Abdiwi et al., 2013; Komeili, 2010; Komeili & Milani, 2013; Sharma et al., 2003) were dedicated to the biaxial deformation of dry fabrics, but very few gave attention to different warp and weft biaxial properties, especially in the context of an objective statistical analysis. Sharma et al., (2003) also provided a force normalization scheme for biaxial testing of fabrics at off-angles, though the fabric behavior still was assumed to be balanced.

From Figure 4.4 the experimental results under pure biaxial mode for the material under study can be seen. For both the warp and weft directions, the normalized axial force increased with displacement. At 1.1 mm displacement, the biaxial forces in the warp and weft direction were 60.7 N/yarn and 78.9 N/yarn, respectively (i. e., ~24% difference). In Figure 4.5 the DIC result of this biaxial deformation has been shown at 78.9 N/yarn biaxial forces for weft direction. The DIC image indicates that the axial displacement at this instant was around 1.08 mm (near to a displacement of 1.1 mm which can be comparable to that in Figure 4.4 for the weft direction under 78.9 N/yarn load). Hence the DIC result gave further confidence in the reliability of the LVDT displacement measurements of the CRN set-up.

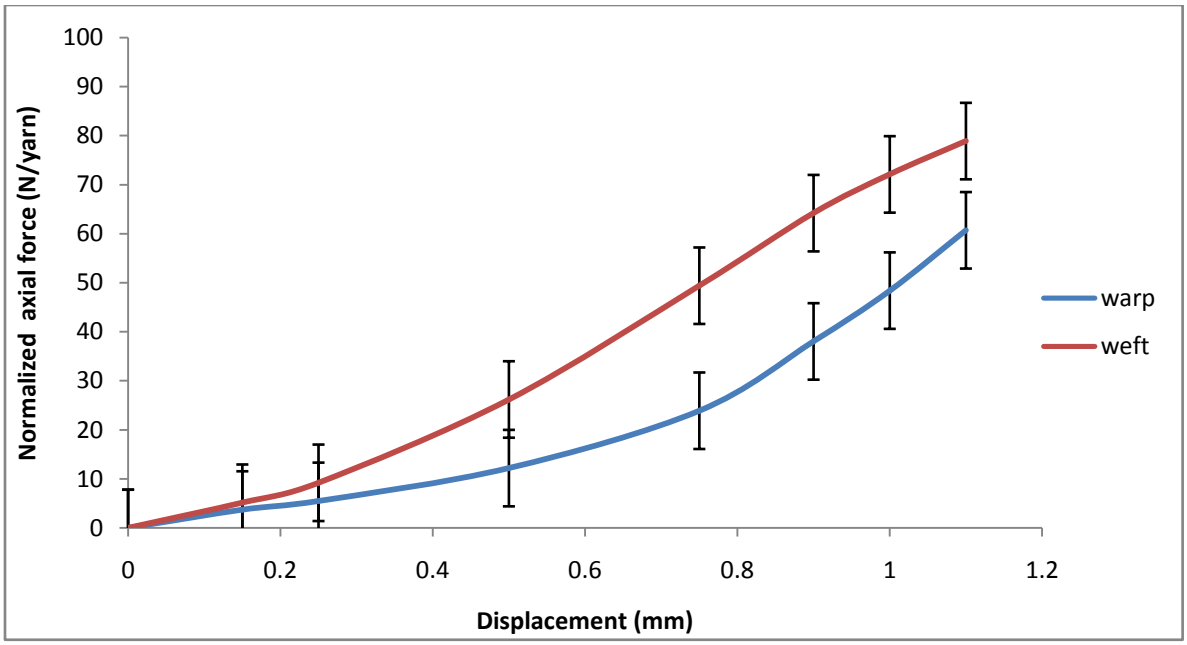

Figure 4.4: Pure biaxial deformation of the Fiberglass fabric in warp and weft directions.

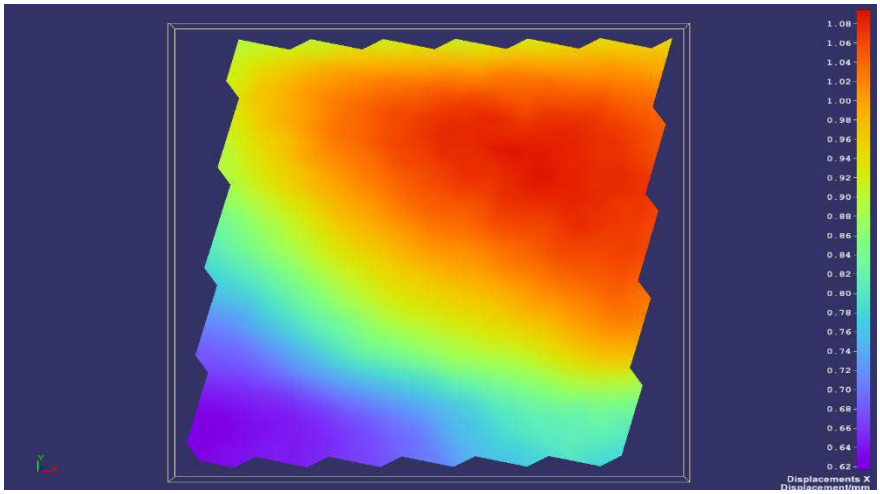

Figure 4.5: Axial displacement measured by using digital image correlation into weft direction.

The statistical analysis of the above pure biaxial test resulted in rejecting the null hypothesis, meaning that the biaxial responses of the warps and wefts are different (P-value 0.008<5%).

4.5 Shear tests

4.5.1 Picture frame shear

The E-Glass TG-54-Nfabric was set under picture frame shear deformation mode that has been received wide interest in the past (Cao et al., 2008; Komeili & Milani, 2013), owing to the fact

that this mode mimics the main deformation mechanism occurring in the draping of fabrics. Figure 4.6 shows the observed picture frame response trend from the CRN machine (please see Section 3.5.3 as to qualitative comparison of shear forces rather than quantitative). Figure 4.6 shows that up to 5^0 of shear angle the two repeated experiments are very close; this is perhaps because at the initial stage of PF test, the noise factors such as misalignment are less effective, and also the shear deformation rate are low.

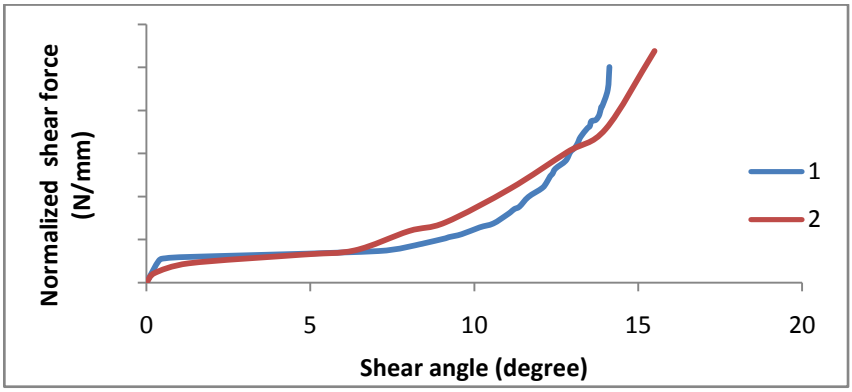

Figure 4.6: Pure picture frame test result of the Fiberglass fabric using CRN instrument.

4.5.2 Circular shear

Using the rotational shear mode of the biaxial–shear CRN machine, a pure circular deformation test was performed. Table 4.2 shows three repeats of the test. The sliding shear angle was measured using a protractor (Figure 4.7) and the sliding or circular shear force was measured by an external load cell manually. The circular shear angle was on average found 10.8^o with an average shear force of 81.76N. Due to the rotation mechanism of yarn, some wrinkling could be seen in the part corner (Figure 4.7).

Table 4.2: Material deformation and uncertainty factors.

Test repeat	Shear angle	Sliding force (N)
1	10^o	79.1
2	10.4^o	80.2
3	12^o	86

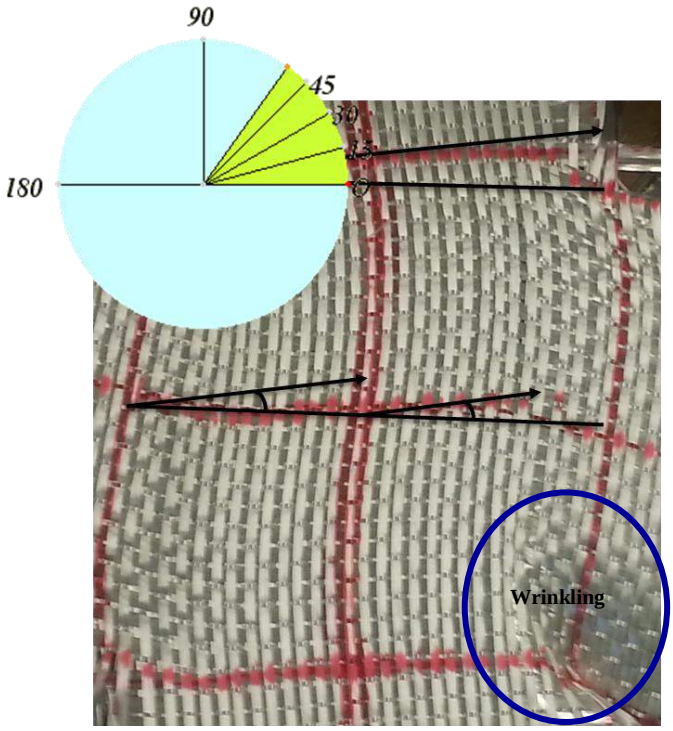

Figure 4.7: The rotational shear angle measurement using a protractor.

4.6 Simultaneous biaxial and shear deformations

Recent researches (Komeili, 2014; Nosrat-Nezami et al., 2014) numerically and experimentally, respectively, presented a simultaneous biaxial-PF shear testing of fabrics, but did not consider the rotational shear effect. The present work conducted two types of simultaneous deformation modes: simultaneous biaxial and picture frame shear; and simultaneous biaxial, picture frame (PF) shear and circular shear (CS). In addition, the earlier efforts did not distinguish between the warp and weft responses under each of these modes.

Experimental test results of the above simultaneous deformation modes shown in Figure 4.8. It can be seen that the simultaneous picture frame shear and biaxial force magnitude (i. e., material resistance to deform) is higher than the simultaneous circular shear, picture frame shear and biaxial loading mode, for both warp and weft directions. Similar to the pure biaxial mode in

Section 4.3, here also the weft response in both simultaneous deformation modes was higher than warp's. The simultaneous PF+biaxial weft response showed the highest axial force per yarn at displacement 1.1 mm. With circular shear affected simultaneous mode, the warp property (blue line in Figure 4.8) showed the lowest value among four combined loading modes, given that the imposed rotation of ~10.8^{o}has caused this family of yarns to experience less tension.

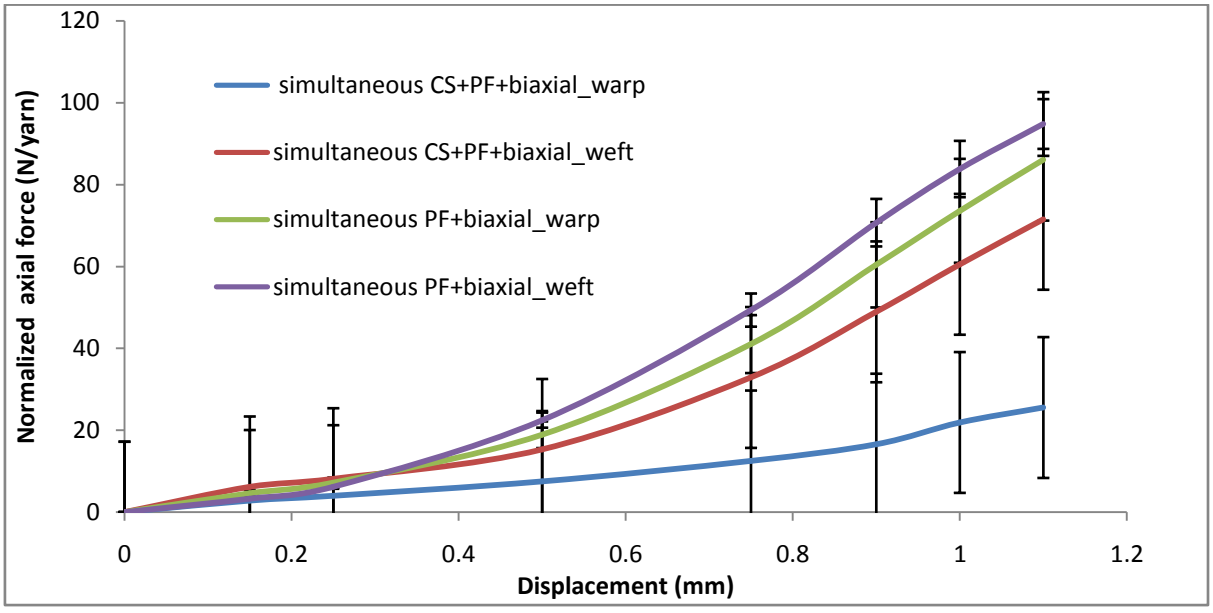

Figure 4.8: Biaxial response of Fiberglass fabrics in warp and weft direction under simultaneous deformation modes in biaxial-shear CRN machine.

During simultaneous deformations of the fabric, the shear response trends were as in Figure 4.9. The shear force trend was found higher for PF+biaxial mode compared to the CS+PF+biaxial mode, though the test could only be performed at low shear angles due to the highly elevated shear stiffness of the fabric in the presence of yarns tension and limited shear load cell capacity.

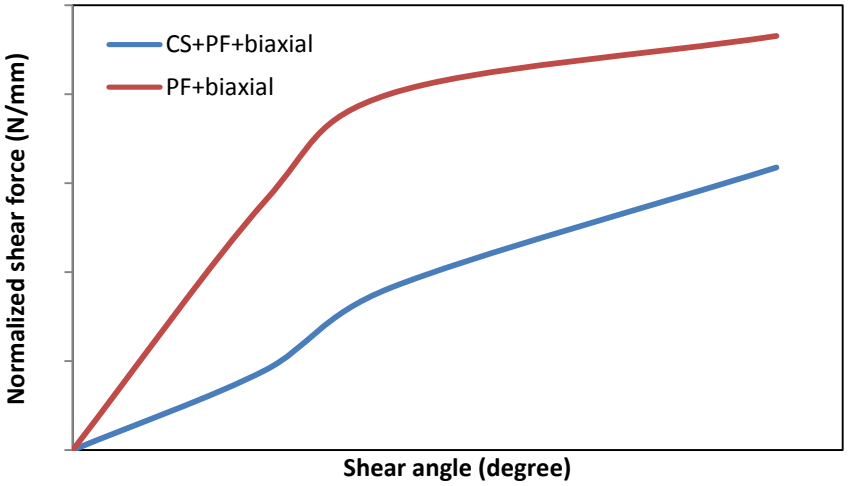

Figure 4.9: Shear response of Fiberglass fabrics under simultaneous deformation modes; at low shear angle regime.

4.7 Coupling evidences

4.8 Comparison between biaxial and simultaneous loading results

Composites undergo multiple loading modes at the same time during forming or actual service in aerospace, automobile and marine fields (e. g., hydrodynamic forces/weight of other sub-components/impacts with external objects, etc.). Hence characterizing the simultaneous biaxial tension, circular and picture frame shear of reinforcement fabrics would be critical to predict the behavior of consolidated final parts (Cavallaro, et al. 2006; Komeili, 2014; Nosrat-Nezami et al., 2014). Combining test data in Sections 4.4 to 4.6, in this section the pure biaxial and simultaneous PF+biaxial modes were compared and analyzed in Figure 4.10.

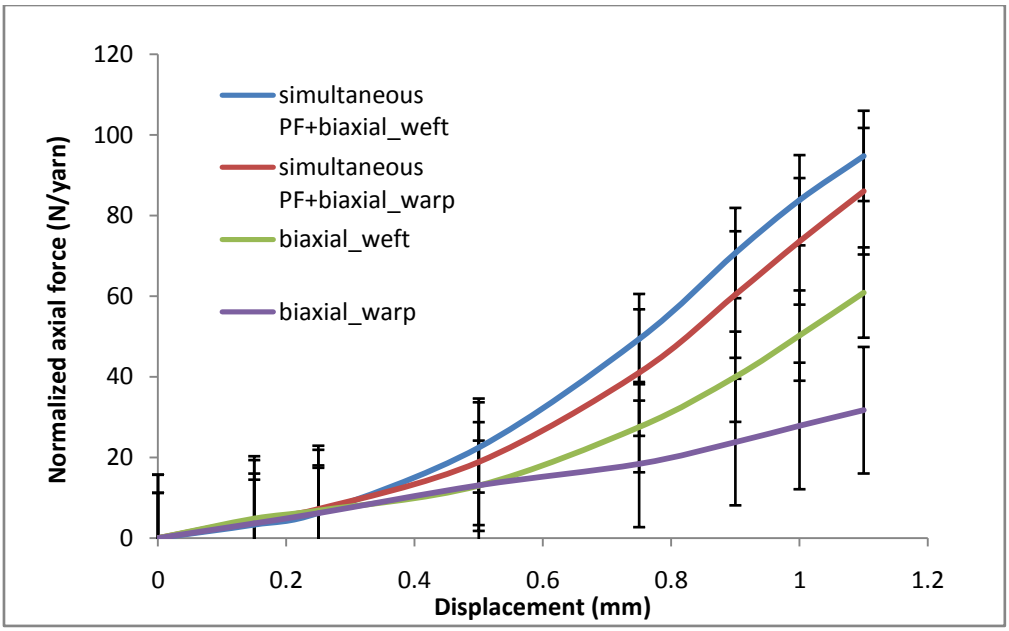

Figure 4.10: Shear-tension coupling study by comparison of simultaneous PF+ biaxial with pure biaxial deformation.

According to Figure 4.10, the yarns behavior under simultaneous shear-tension was found to be much higher than that in the pure biaxial mode. In addition, weft yarns for both pure and simultaneous loading modes show a higher axial force that warp; also note from the material specifications, Table 3.1, that the warp end count of 8 per cm which is lower than the weft end count (11 per cm); Figure 3.16 also showed that warp yarns are normally more wavy than the weft yarns.

Next, ANOVA analysis was performed to statistically observe the above experimental differences. From the hypothesis testing between the simultaneous PF+biaxial and pure biaxial modes, for the weft axial property the P-value was found to be 0.03, and for the warp direction it was 0.025. These values mean that the null hypothesis can be rejected, indicating that in applying shear while tensioning the yarns, their axial stiffness are significantly changing (i. e., coupling effect of shear on tensile behavior of the fabric).

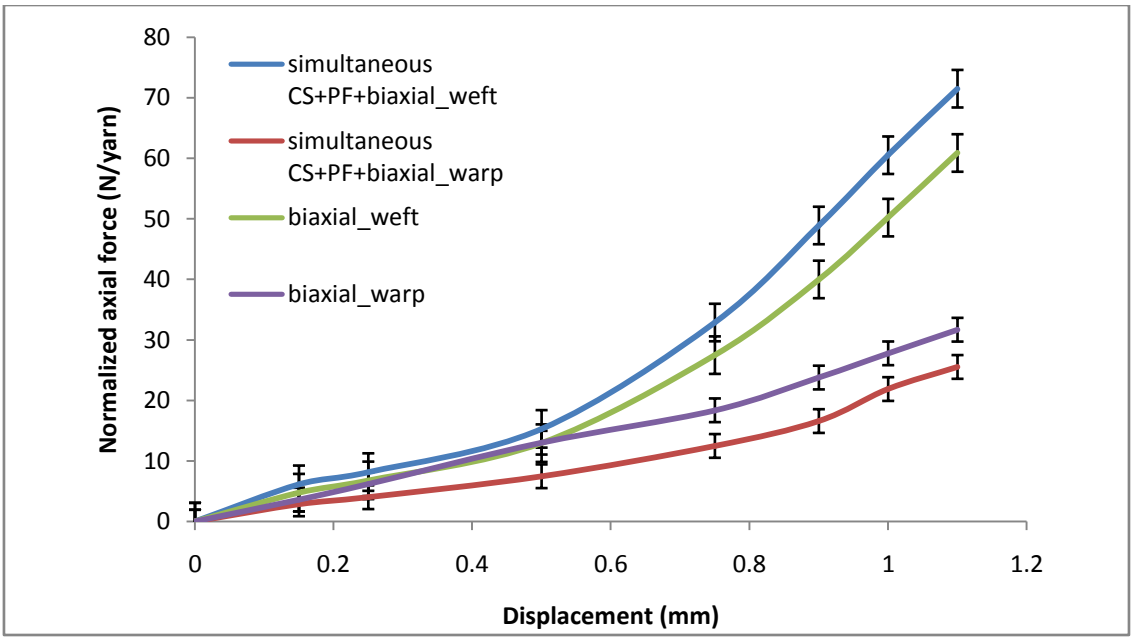

Figure 4.11: Shear-tension coupling study by comparison of simultaneous CS+PF+ biaxial with pure biaxial deformation.

Next a similar coupling analysis was performed between the pure biaxial mode and simultaneous CS+PF+bixial mode. According to Figure 4.11, shear-tension coupling in simultaneous CS+PF+ biaxial is found to be the highest in weft direction. However, the warp axial force was lower for simultaneous CS+PF+biaxial than pure biaxial mode. The reason of that was that during the latter test, the circular shear (rotation) was applied to warp yarns, hence CS+PF+biaxial warp was at a larger angle with the corresponding motor normal force direction.

ANOVA analysis between the above two deformation modes were carried out for both warp and weft directions. The null hypotheses were rejected in both cases as P-value was found to be 0.014 for weft yarns and 0.001 for the warp yarns, respectively. ANOVA analysis concluded that the combined PF+CF shear modes significantly affect the biaxial response of the fabric and hence a severe coupling exists.

4.9 A sequential coupling mode: PF shear followed by biaxial tension

During the molding of fabrics, they may experience some tension or shear sequentially depending on how the manufacturing process is designed by engineers (e. g., handling of fabrics before molding may induce some pre-shear, whereas the installment of the fabric in a blank-holder may induce some pre-tension). The present research has conducted two types of sequential coupling tests. This sub-section presents the case of pre- shear followed by biaxial deformation. Here, the dry non-crimp fabric experienced 15^{o} picture frame shear by the instrument and then undertook the biaxial tension. Figure 4.12 illustrates such sequential shear-tension coupling results, both regarding warp and weft behaviors.

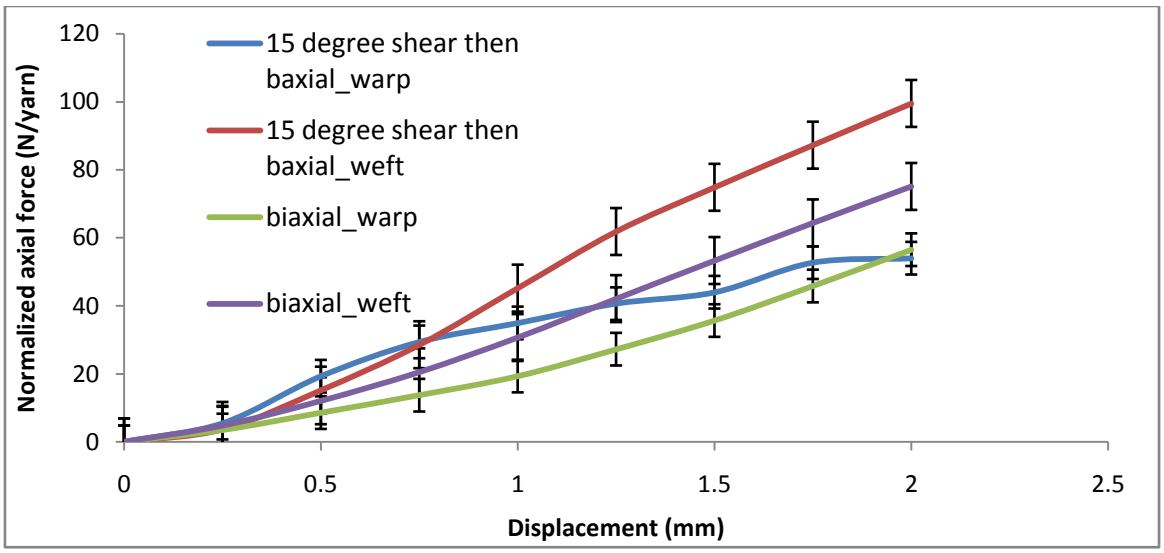

Figure 4.12: Sequential coupling study (15^{o} shear then biaxial) and its comparison with pure biaxial deformation.

The 15^{o} sheared then biaxial tensioned coupled fabric overall, showed higher tensile forces than the pure biaxial mode in the weft and warp directions. Between the shear affected biaxial mode and pure biaxial mode a two-way ANOVA was also performed. The P-value in the weft direction was 1.36E-5 and in the warp direction it was 0.008, which means the corresponding null

hypotheses were rejected and the pre-shear has indeed an effect on both warp and weft responses of the material.

4.10 Sequential biaxial followed by PF shear

The other sequential coupling test performed in this thesis was pre-biaxial tension followed by shear. Namely, 1000 N biaxial tension was applied to the fabric and then the pre-tensioned fabric went through picture frame shear mode. The sequential mode resulted in a higher shear force trend than the pure picture frame shear as shown in Figure 4.13.

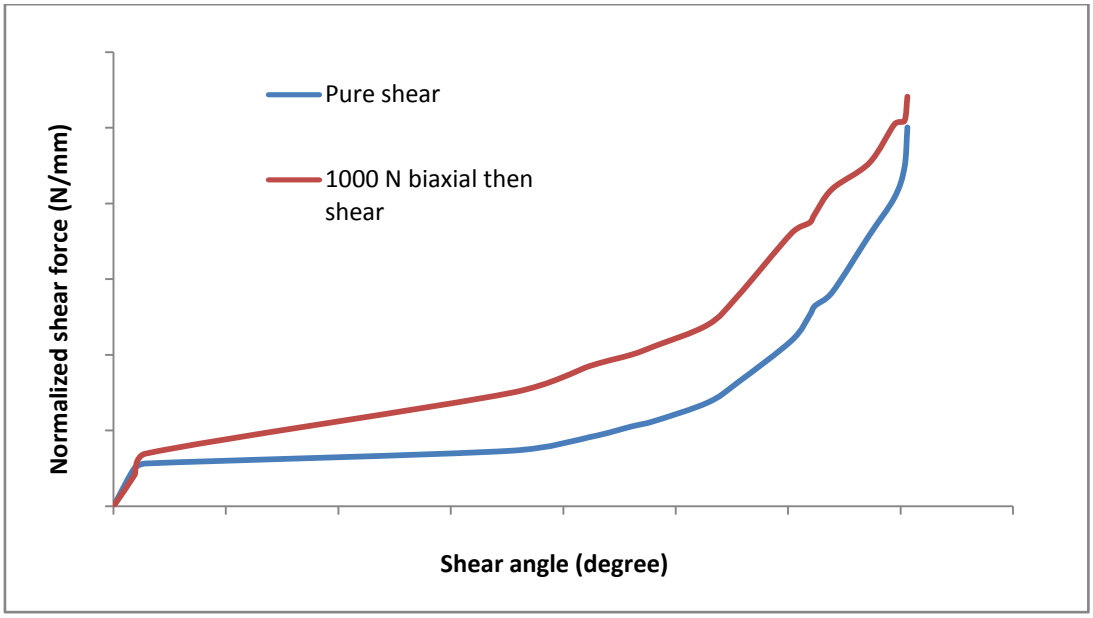

Figure 4.13: Qualitative comparison of sequential biaxial-shear mode and the pure biaxial mode.

4.11 Comparison between pure shear and tension affected shear

Figure 4.14 shows a general comparison of pure picture frame shear versus simultaneous circular shear-picture frame shear-biaxial tension response of the Fiberglass non-crimp fabric. The rate of biaxial deformation was much faster than the shear response in such simultaneous experiments and for that reason the shear angles monitored were very small before the maximum elongation limit is reached. Regardless, simultaneous (coupled) deformation mode from the beginning of deformation showed a higher shear response than the pure shear response. Figure 4.15 shows the

simultaneous PF+biaxial shear response versus the pure picture frame mode, again conforming that the tension in yarns affects the shear behavior (and hence the drapability) of the fabric.

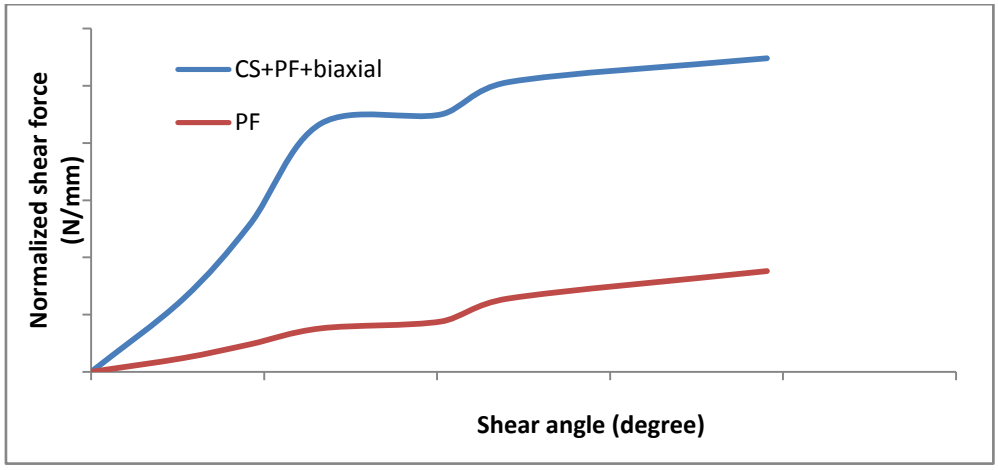

Figure 4.14: Qualitative comparison of the shear response of the fabric under the pure picture frame and simultaneous CS+PF+biaxial modes; at low shear angle regime.

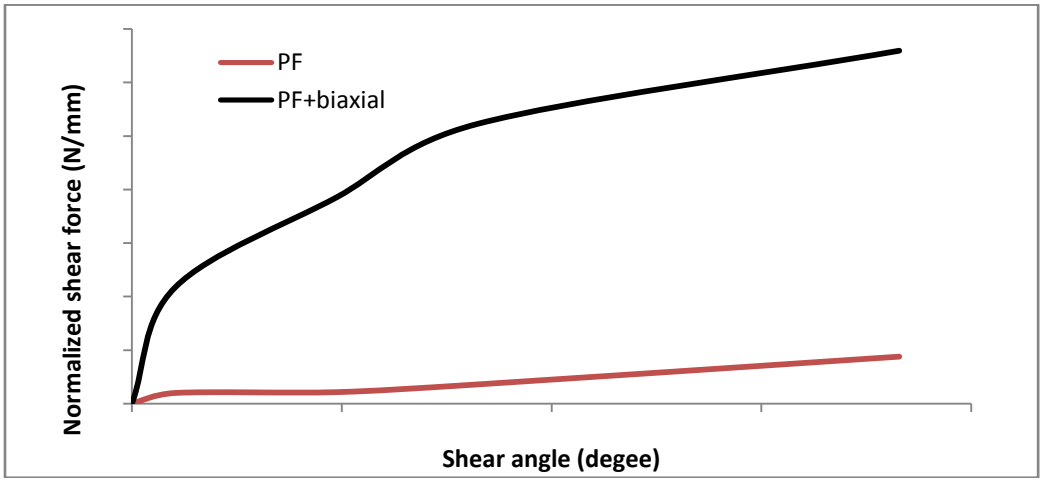

Figure 4.15: Qualitative comparison of the shear response of the fabric under the pure picture frame and simultaneous PF+biaxial modes; at low shear angle regime.

4.12 Coupling factor

Nosrat-Nezami and his colleagues recently defined a coupling factor by using the ratio of coupled and uncoupled shear force responses of the fabric (Nosrat-Nezami et al., 2014). The current work similarity defined a coupling factor in the sequential case of 1000N biaxial, then shear deformation in comparison to the pure shear (i. e., when the biaxial load is zero):

coupling Factor $(CF) = \frac{Fs\,(1000\,N)(\gamma)}{Fs\ (0N)(\gamma)}$. According to Figure 4.16, the coupling effect in the glass fiber fabric increases as the shear angle increases, and then it starts decreasing. This trend exactly matches the one observed by (Nosrat-Nezami et al., 2014) for carbon fiber fabrics.

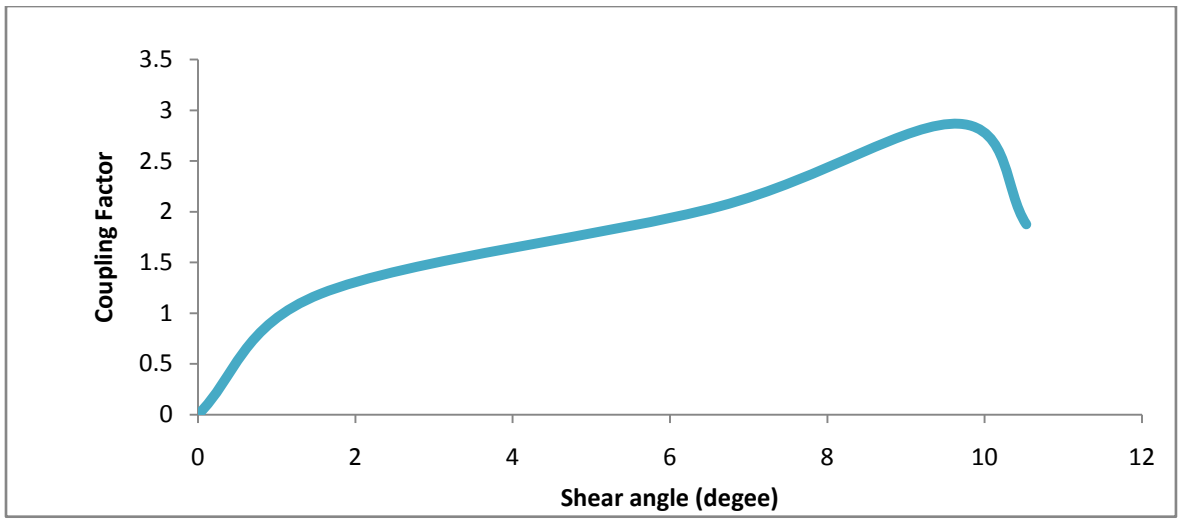

Figure 4.16: General trend observed for shear-tension coupling effect as a function of shear angle.

Coupling factor can be similarly calculated by for simultaneous modes: $CS = \frac{Fs,simultaneous\ \ (\gamma)}{Fs,pure\ \ PF\ (\gamma)}$. The general expected trend is shown in Figure 4.17, where we speculate that without yarn sliding (i. e., without CS), a much higher coupling factor is present in the fabric; this remains as a worthwhile future study to confirm and comprehend its roots, e. g., using a meso-level finite element model.

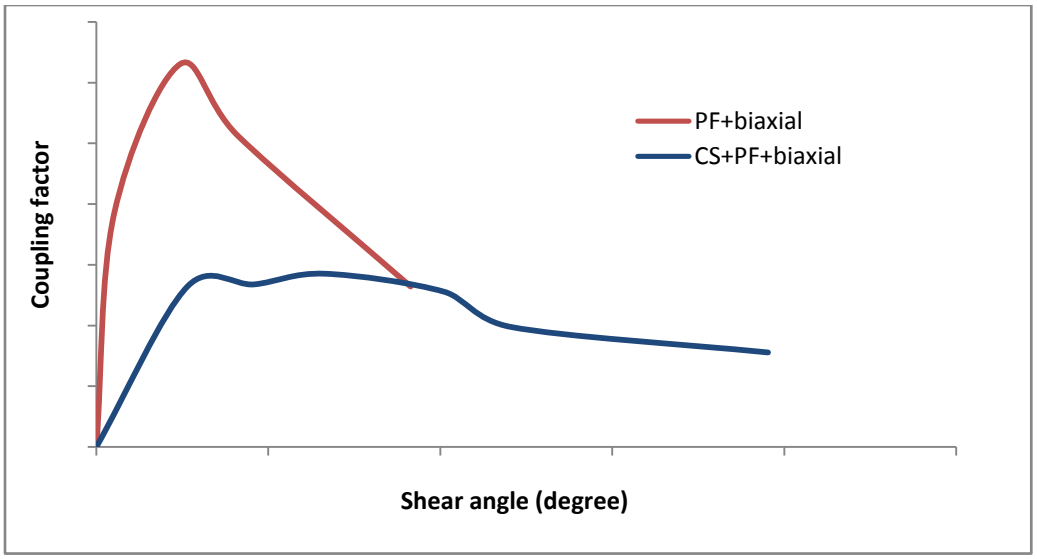

Figure 4.17: Coupling factor for simultaneous deformation modes.

4.13 Deformed samples in the coupling tests

Before start of each test, square lines had been marked on each sample to monitor changes after deformation in the region of interest, as shown in Figure 4.18. As can be seen in Figure 4.18, there are signs of deformation noises such as fiber misalignment, fiber slippage, etc. At applying 1000 N biaxial then shear, the deformed area looks like a uniform rhomboid surface (Figure 4.18(a)). Some green line movement from the square box area towards the loading direction (indicating fiber putt-out) can be seen in Figure 4.18(b). When picture frame shear and biaxial tension is applied at same time (Figure 4.18(c)), the fibers at the boundary of region of interest tend to move simultaneously along the tensile loading direction and diagonally across the frame movement. With the increase of biaxial loading and shear force, fibers further deform and finally at ~2500N biaxial load at some places of the fabric the fiber become torn. Yarn sliding is a direct consequence of forced fiber rotation from warp toward weft under the circular shear mode. Accordingly, under simultaneous circular shear, picture frame shear and biaxial tension mode the deformation complexity/non-uniformity and fabric tearing became most obvious (Figure 4.18(d)). In fact according to the circular shear contribution in this mode the crossover points of

red mark lines are not coincident after deformation any more, which well mimics the theoretical scheme in Figure 3.10.

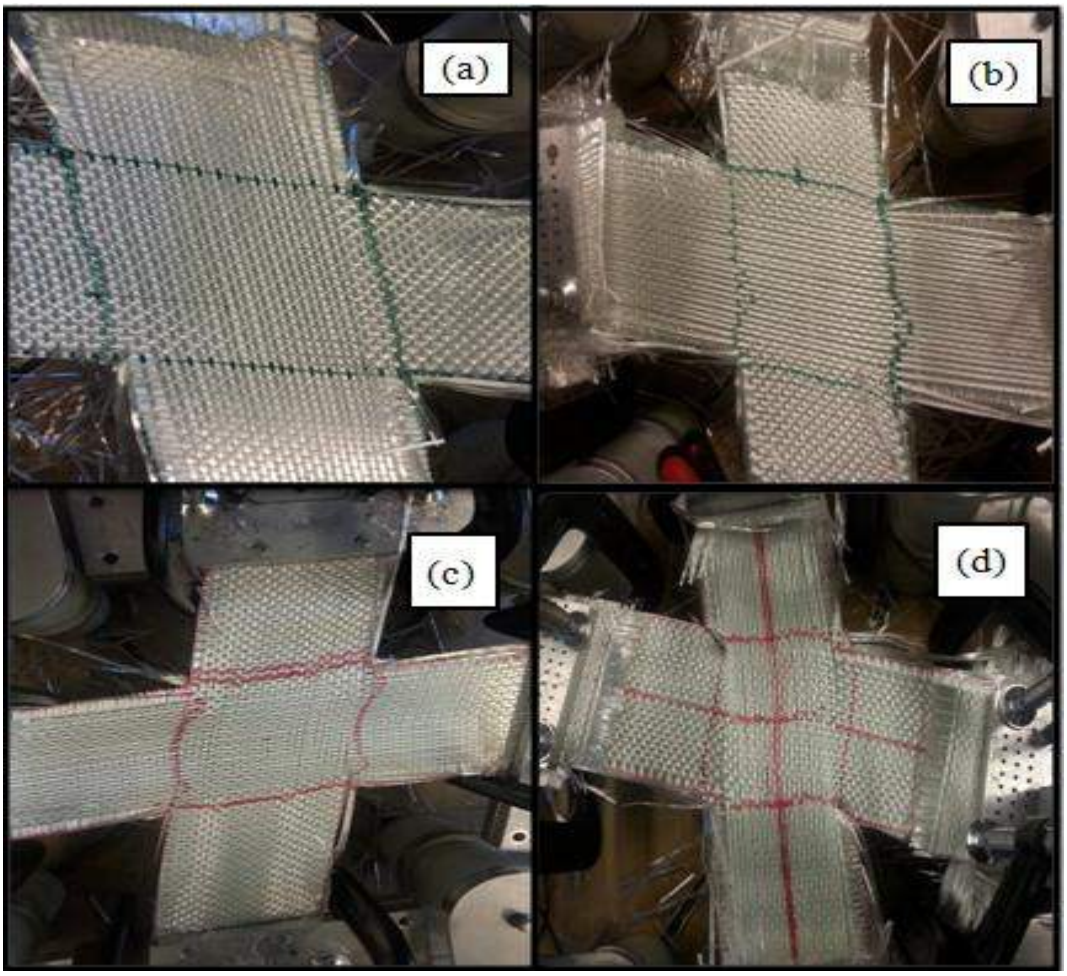

Figure 4.18: Deformed fabric samples after different types of tests (a) 1000N biaxial, then shear, (b) 15^{o} shear then biaxial, (c) simultaneous biaxial and PF shear, (d) simultaneous circular shear, picture frame shear and biaxial.

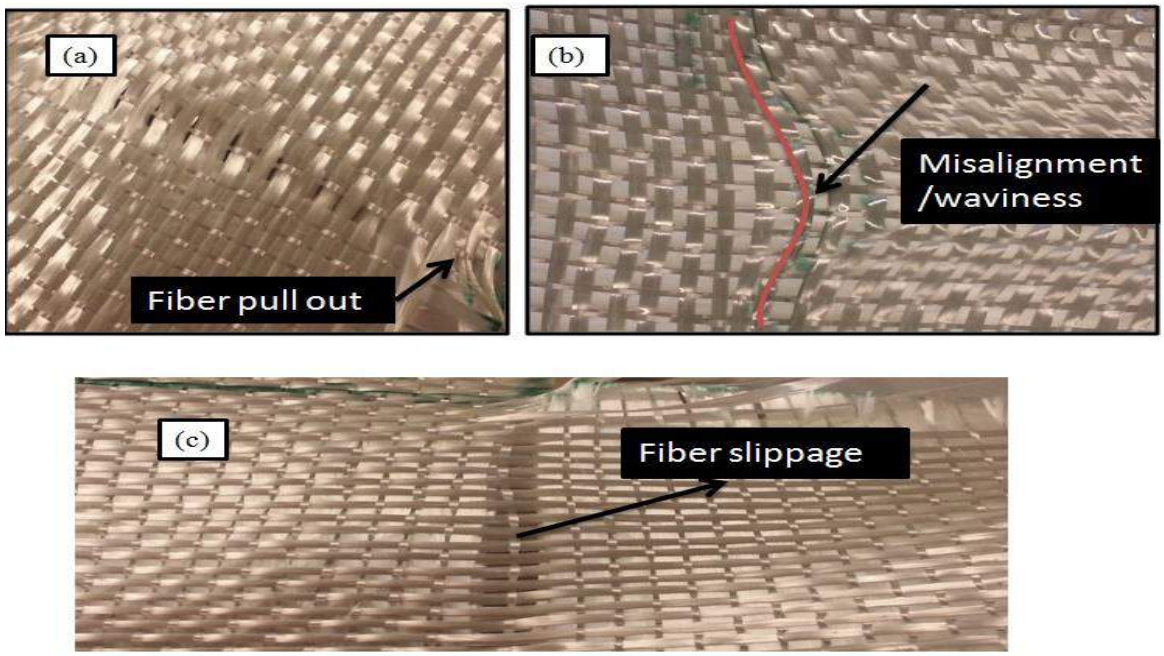

Figure 4.19: Example of deformation defects observed in the Fiberglass non-crimp fabric under combined loading tests.

Inside the inner deformation area, further zoomed-in examples of defects under simultaneous loading conditions are illustrated in Figure 4.19. In Figure 4.19(a), fiber pull-out is seen when a weft yarn has been under an excessive loading of ~2500 N. Due to initial misalignment in the fabric and/or deviation from theoretical ideal clamping condition and subsequent pull-out, yarn waviness has formed (Figure 4.19(b)). The misaligned deformation direction is aligned with the biaxial loading direction. Another very common defect, fiber slippage that is often observed during the experimentation on non-crimp fabrics is shown in Figure 4.19(c). Only when the axial deformation of yarns was reaching to its extreme stages, fiber slippage was visible in the fabric.

4.14 Out-of-plane wrinkle test

In 2012 Harrison investigated the onset of wrinkling of a jute woven fabric by using backlit imaging during bias extension tests (Harrison, 2012). The current research used digital image correlation (DIC) to observe wrinkling (Figure 4.20). The dry woven fabrics are often loose

before consolidation stage and hence any misalignment or mishandling of the fabric during installation in the test frame can cause early wrinkles. Conversely, non-crimp fabrics are straight and often stiffer than woven fabrics. Nevertheless, during sample preparation, handling, or loose clamping there can be a chance of possible yarn misalignment and wrinkling. Under some tension in yarns, such wrinkles were literally absent as can be seen in Figures 4.18(a) and 4.18(c). The latter was additionally verified quantitatively via the DIC as follows.

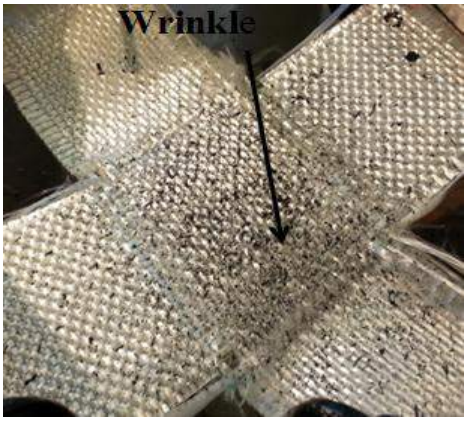

Figure 4.20: Out of plane wrinkling observed during picture frame shear test.

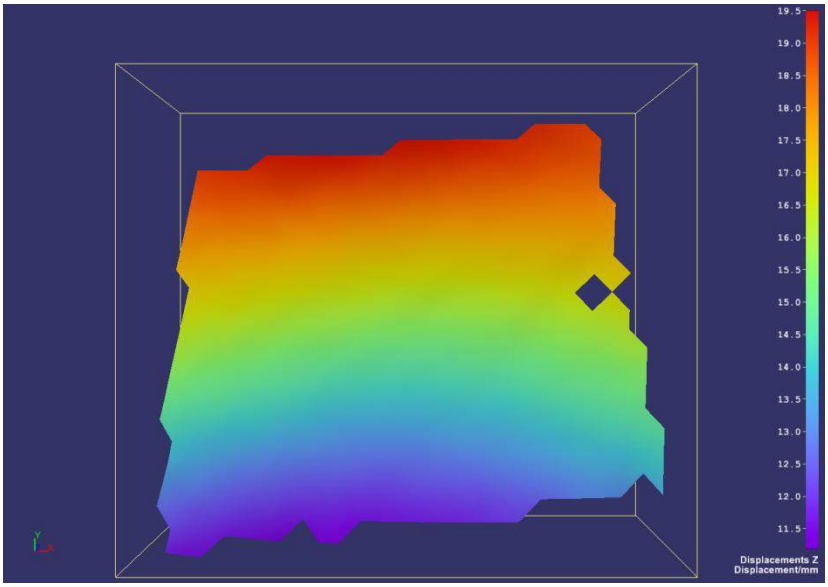

Figure 4.21: Wrinkle formation of the Fiberglas fabric during shear, as recorded by DIC.

As explained in Section 3.6.2, during a picture frame shear of the Fiberglass fabric, the sample was previously made ready for DIC recording with a speckle pattern. During image analysis, Z direction displacements above ~4mm were considered as wrinkles. Subsequent processing of the imaging data by DIC (Figure 4.21), showed that the Z direction displacement in this test was between 11.5mm to 19.5 mm at $8^{o}$of shear angle, which indicated a slightly wrinkled specimen out-of-plane. However, when applying simultaneous biaxial and picture frame shear, the magnitude of displacement in the Z direction by DIC was found to be very low (~0.6 mm) at a comparable shear angle (Figure 4.22).

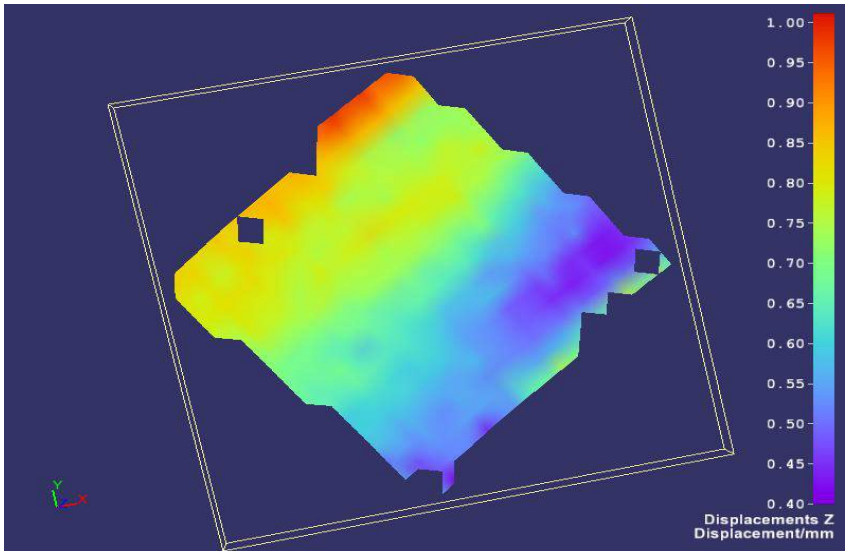

Figure 4.22: Out-of-plane deformation/wrinkling disappearance during simultaneous PF shear and biaxial test.

Simultaneous tension-shear with free rotation of boundary condition has caused much lower magnitude of Z direction wrinkles.

4.15 Summary

This chapter presented the experimental findings on a Fiberglass non-crimp fabric under different individual and combined loading modes. From statistical results of the analyses it is

clear that the shear-tension coupling under both simultaneous and sequential combined loading modes can necessitate higher forces for further deformation of the fabric, indicating stiffening of both axial and shear rigidity of the material. The coupling effect can also induce some non-uniform deformation distributions and early damage/defects in the sharp edges of the forming material. Simultaneous PF+biaxial mode can reduce wrinkling during forming process.

Chapter 5: Conclusion and Future Work

A majority of past works in the analysis of fabric composites had assumed tension and shear deformation modes in a decoupled form; however, this has been questioned recently by means of numerical simulations (e. g., Komeili, 2014) as well as experimental evidences(e. g., Nosrat-Nezami et al., 2014). Therefore, this research project was aimed to further assess the tension-shear coupling effect and contributed to ongoing efforts toward a full characterization and standardization of test methods for forming of composite materials. The statistical analysis throughout the tests was found very useful to confirm the reliability of experimental observations. Table 5.1 presents the summary of the ANOVA analysis results for different combined loading modes tested, as each is related to a different coupling aspect of shear-tension in fabrics.

Table 5.1: Summary of the ANOVA analyses of different combined loading modes.

Deformation modes tested for the null hypothesis	**Conclusion**
Biaxial vs. simultaneous biaxial+ PF	Simultaneous shear-tension loading is significantly affecting the response of both yarn families (P-weft 0.025, P-warp 0.03).
Biaxial vs. Simultaneous CS + PF+ biaxial	Simultaneous shear-tension loading with addition, fiber rotation (mimicking sliding) is significantly affecting the response of both yarn families (P-weft 0.014, P-warp 0.001)
Simultaneous PF+ biaxial vs. simultaneous CS+PF+biaxial	The rotational shear mode is significantly affecting the coupling behavior in biaxial-shear mode (P-weft 0.03, P-warp 0.022).
Biaxial with 15 degree pre-PF shear vs. pure biaxial	Pre-shear is significantly affecting the biaxial deformation of yarns (P-weft 1.36 E-5, P-warp 0.008).
Pure PF shear vs. 1000 N pre-biaxial tension, then shear	Pre-tension is significantly affecting the shear deformation of yarns (qualitatively shown)

In addition, ANOVA results under other individual modes and their comparisons revealed that:

1. For both uniaxial and biaxial deformation modes the warp and weft yarn properties are significantly different (unbalanced fabric behavior).
2. The biaxial and uniaxial behaviors in a given yarn direction is significantly different, indicating the weft-warp interaction dependency on deformation mode (state of deformation) in composites.
3. Weft yarns were stiffer than warp yarns in their axial response under several deformation modes.
4. Simultaneous PF+biaxial mode showed higher normal force per yarn and coupling factor than CS+PF+biaxial.
5. The expected shear force order is: Pure PF<CS+PF+biaxial<PF+biaxial<1000N pre-biaxial then shear.
6. Under tension of yarns, wrinkles were literally absent during shearing of the fabric as verified visually and quantitatively by DIC.

5.1 Limitations of the work

The main limitation of the work was the challenge in measurement and calibration of PF shear force, in particular given the horizontal set-up of the test fixture (Figure 3.23) and hence a high effect from frictional forces. In addition, all tests were performed at room temperature and quasi-static loading rates. In fast forming processes, or impact /ballistic applications, the fabric will deform and damage much faster.

5.2 Future work recommendations for practical application of this thesis

Fiberglass and carbon fiber woven and non-woven composite parts are more and more used in aerospace, automotive, and naval applications (Cavallaro, 2015). Defects such as wrinkling is

critical for designers in these industries during forming of fabrics (see, e. g., a draping set-up in Figure 5.1), and this requires a very careful characterization of different fiber reinforcements. The newly designed biaxial-shear test set-up at CRN may be further improved (especially regarding the shear load calibration) and used in this industrial research direction, especially to help manufacturers move toward a tension-assisted shearing/draping of fabrics during forming, without encountering other side defects such as pre-mature fiber failure, etc. In addition, the characterization results may be used in conjunction with future simulations of fabrics during draping, in the presence of coupling effects. The reliability of simulations in turn will result in better prediction and minimization of membrane stresses in composite layers during forming processes. During manufacturing of complex shapes, defects such as wrinkling often occur in corner areas (Lightfoot et al. 2013). The present research results may be helpful for a better characterization and prevention of wrinkles in these areas by providing pretention to the fabric during molding set-up design.

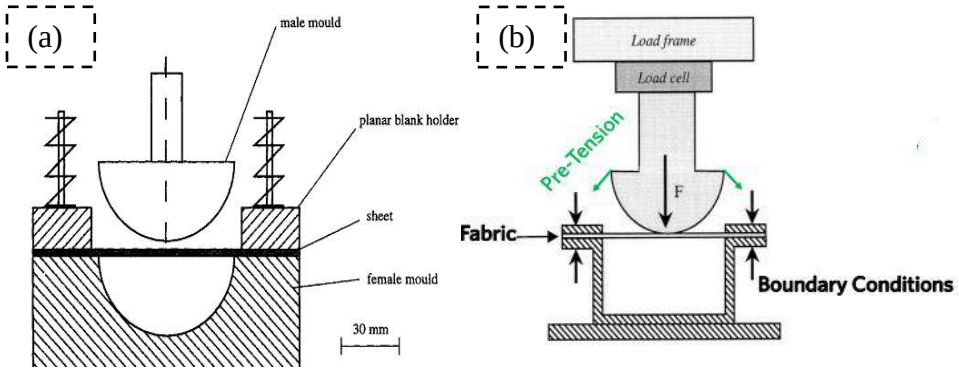

Figure 5.1: Future work outlook: By characterizing tension assisted shearing of fabrics, an optimum level of membrane pre-stress may be generated in the yarns by blank holders/mold geometry modifications to prevent wrinkles during draping; (a) original industrial draping set-up (Breuer et al., 1996), (b) suggested design for future work (Rashidi et al., 2015).

Bibliography

Abdiwi, F., Harrison, P., & Yu, W. (2013). Modelling the Shear-Tension Coupling of Woven Engineering Fabrics. *Advances in Materials Science and Engineering,* Article ID 786769.

Ardakani, M. A., Khatibi, A. A., & Ghazavi, S. A. (2008). *A study on the Manufacturing of Glass-Fiber-Reinforced Aluminum Laminates and the Effect of Interfacial Adhesive Bonding on the Impact Behavior*. *t*he Proceedings of the XI International Congress and Exposition.

Aymerich, F., & Meili, S. (2000). Ultrasonic evaluation of matrix damage in impacted composite laminates. *Composites Part B: Engineering, 31*(1), 1-6.

Bilisik, K. (2011). Pull-out properties of polyester woven fabrics: effects of softening agent and interlacement on single and multiple yarn pull-out forces and analysis by statistical model. *Fibers and Polymers, 12*(8), 1106-1118.

Bilisik, K., & Yolacan, G. (2012). Experimental determination of bending behavior of multilayered and multidirectionally-stitched E-Glass fabric structures for composites. *Textile Research Journal, 82*(10), 1038-1049.

Bloom, L., Wang, J., & Potter, K. (2013). Damage progression and defect sensitivity: An experimental study of representative wrinkles in tension. *Composites Part B: Engineering, 45*(1), 449-458.

Boisse, P., Borr, M., Buet, K., & Cherouat, A. (1997). Finite element simulations of textile composite forming including the biaxial fabric behaviour. *Composites Part B: Engineering, 28*(4), 453-464.

Boisse, P., Hamila, N., Vidal-Sallé, E., & Dumont, F. (2011). Simulation of wrinkling during textile composite reinforcement forming. Influence of tensile, in-plane shear and bending stiffnesses. *Composites Science and Technology, 71*(5), 683-692.

Breuer, U., Neitzel, M., Ketzer, V., & Reinicke, R. (1996). Deep drawing of fabric-reinforced thermoplastics: Wrinkle formation and their reduction. *Polymer Composites, 17*(4), 643-647.

Buet-Gautier, K., & Boisse, P. (2001). Experimental analysis and modeling of biaxial mechanical behavior of woven composite reinforcements. *Experimental Mechanics, 41*(3), 260-269.

Cao, J., Akkerman, R., Boisse, P., Chen, J., Cheng, H., De Graaf, E., et al. (2008). Characterization of mechanical behavior of woven fabrics: experimental methods and benchmark results. *Composites Part A: Applied Science and Manufacturing, 39*(6), 1037-1053.

Carvelli, V., Corazza, C., & Poggi, C. (2008). Mechanical modelling of monofilament technical textiles. *Computational Materials Science, 42*(4), 679-691.

Cavallaro, P. V., Johnson, M. E., & Sadegh, A. M. (2003). Mechanics of plain-woven fabrics for inflated structures. *Composite Structures, 61*(4), 375-393.

Cavallaro, P. V., Quigley, C. J., Johnson, A. R., & Sadegh, A. M. (2004). *Effects of Coupled Biaxial Tension and Shear Stresses on Decrimping Behavior in Pressurized Woven Fabric.* Paper presented at the ASME 2004 International Mechanical Engineering Congress and Exposition.

Cavallaro, P. V. (2015). Effects of weave styles and crimp gradients in woven kevlar/epoxy composites. *Experimental Mechanics* (in press).

Cavallaro, P. V., Sadegh, A. M., Quigley, C. J., & Johnson, A. R. (2006). Effects of Coupled Biaxial Tension and Shear Stresses on Decrimping Behavior in Pressurized Woven Fabrics. *Technical report: Naval Undersea Warfare Center Division New Port, Rhode Island.*

Cavallaro, P. V., Sadegh, A. M., & Quigley, C. J. (2007). Decrimping behavior of uncoated plain-woven fabrics subjected to combined biaxial tension and shear stresses. *Textile Research Journal, 6*(77).

Chen, F. M., Wang, G., Jiang, Z. H., Cheng, H. T., Chen, X. M., Yu, Z. X., & Zhang, W. F. (2011). A Novel 3-D Testing System for the Mechanical Properties of Fiber Fabrics and Textile Composites. *Advanced Materials Research, 332*, 1206-1209.

Chen, J., Lussier, D., Cao, J., & Peng, X. (2001). Materials characterization methods and material models for stamping of plain woven composites. *International Journal of Forming Processes, 4*, 269-284.

Çınar, K., & Ersoy, N. (2015). Effect of fibre wrinkling to the spring-in behaviour of L-shaped composite materials. *Composites Part A: Applied Science and Manufacturing, 69*, 105-114.

Collier, B. J. (1991). Measurement of fabric drape and its relation to fabric mechanical properties and subjective evaluation. *Clothing and Textiles Research Journal, 10*(1), 46-52.

Colman, A. G., Bridgens, B. N., Gosling, P. D., Jou, G.-T., & Hsu, X.-Y. (2014). Shear behaviour of architectural fabrics subjected to biaxial tensile loads. *Composites Part A: Applied Science and Manufacturing, 66*, 163-174.

Conor, P., James, A., Hollis, M., & Campbell, S. (2012). Applications of fractography for aircraft defect causal analysis. *Fatigue & Fracture of Engineering Materials & Structures, 35*(1), 84-91.

Creech, G., & Pickett, A. K. (2006). Meso-modelling of non-crimp fabric composites for coupled drape and failure analysis. Journal of materials science, 41(20), 6725-6736.

da Silva Junior, J., Paciornik, S., & d'Almeida, J. (2004). Evaluation of the effect of the ballistic damaged area on the residual impact strength and tensile stiffness of glass-fabric composite materials. *Composite structures, 64*(1), 123-127.

De Bilbao, E., Soulat, D., Hivet, G., & Gasser, A. (2010). Experimental study of bending behaviour of reinforcements. *Experimental mechanics, 50*(3), 333-351.

De Morais, W., Monteiro, S., & d'Almeida, J. (2005). Evaluation of repeated low energy impact damage in carbon–epoxy composite materials. *Composite Structures, 67*(3), 307-315.

Deborah A. p. Hersman, R. L. S., Christopher A. Hart , mark R. Rosekind, earl F. Weener. (2013). Rapid Decompression Due to Fuselage Rupture, Southwest Airlines Flight 812.

Edgren, F., Mattsson, D., Asp, L. E., & Varna, J. (2004). Formation of damage and its effects on non-crimp fabric reinforced composites loaded in tension. Composites Science and Technology, 64(5), 675-692.

El-Sabbagh, A., & Taha, I. (2013). Characterization of the draping behavior of jute woven fabrics for applications of natural-fiber/epoxy composites. *Journal of Applied Polymer Science, 130*(3), 1453-1465.

Elliot , B., Dan, L., Mendel, N., Bhoome, P., & Matthew, R. (2012). *Stand-Alone Desktop Biaxial And Shear Testing Fixture,* Capstone Project Report, City College of New York.

Flores-Johnson, E., Carrillo, J., Gamboa, R., & Shen, L. (2014). Experimental and Numerical Study of Plain-Woven Aramid Fabric. *Advanced Materials Research, 856*, 74-78.

Fong, L., & Advani, S. (1994). The role of drapability of fiber preforms in resin transfer molding: Technomic Publishing Co., Inc., Lancaster, PA (United States).

Gasser, A., Boisse, P., & Hanklar, S. (2000). Mechanical behaviour of dry fabric reinforcements. 3D simulations versus biaxial tests. *Computational Materials Science, 17*(1), 7-20.

Gereke, T., Döbrich, O., Hübner, M., & Cherif, C. (2013). Experimental and computational composite textile reinforcement forming: A review. *Composites Part A: Applied Science and Manufacturing, 46*, 1-10.

Guagliano, M., & Riva, E. (2001). Mechanical behaviour prediction in plain weave composites. *The Journal of Strain Analysis for Engineering Design, 36*(2), 153-162.

Gujjala, R., Ojha, S., Acharya, S., & Pal, S. (2014). Mechanical properties of woven jute–glass hybrid-reinforced epoxy composite. *Journal of Composite Materials, 48*(28), 3445-3455.

Hamila, N., & Boisse, P. (2008). Simulations of textile composite reinforcement draping using a new semi-discrete three node finite element. *Composites Part B: Engineering, 39*(6), 999-1010.

Hancock, S., & Potter, K. (2006). The use of kinematic drape modelling to inform the hand lay-up of complex composite components using woven reinforcements. *Composites Part A: Applied Science and Manufacturing, 37*(3), 413-422.

Harrison, P. (2012). Normalisation of biaxial bias extension test results considering shear tension coupling. *Composites Part A: Applied Science and Manufacturing, 43*(9), 1546-1554.

Harrison Philip , A. F., Guo Z. , Potluri P., yu W. r. . (2012). Characterising the shear–tension coupling and wrinkling behaviour of wovenengineering fabrics. *Composites: Part A, 43*, 903-914.

Hayman, B., Berggreen, C., & Pettersson, R. (2007). The effect of face sheet wrinkle defects on the strength of FRP sandwich structures. *Journal of Sandwich Structures and Materials, 9*(4), 377-404.

Hayman, B., Echtermeyer, A., & McGeorge, D. (2001). *Use of Fibre Composites in Naval Ships. t*he Proceedings of Warship-International Conference.

Hsiao, H., & Daniel, I. (1996). Effect of fiber waviness on stiffness and strength reduction of unidirectional composites under compressive loading. *Composites Science and Technology, 56*(5), 581-593.

Işık, B., & Ekici, E. (2010). Experimental investigations of damage analysis in drilling of woven glass fiber-reinforced plastic composites. *The International Journal of Advanced Manufacturing Technology, 49*(9-12), 861-869.

Jackson, A. L., Bridgens, B. N., & Gosling, P. D. (2010). *A New Biaxial And Shear Protocol for Architectural Fabrics. t*he Symposium of the International Association for Shell and Spatial Structures (50th. 2009. Valencia).

Kawabata, S., & Niwa, M. (1989). Fabric performance in clothing and clothing manufacture. *Journal of the Textile Institute, 80*(1), 19-50.

Kawabata, S., Niwa, M., & Kawai, H. (1973a). 3—The finite-deformation theory of plain-weave fabrics part I: the biaxial-deformation theory. *Journal of the Textile Institute, 64*(1), 21-46.

Kawabata, S., Niwa, M., & Kawai, H. (1973b). 4—The finite-deformation theory of plain-weave fabrics. Part II: the uniaxial-deformation theory. j*ournal of the Textile Institute, 64*(2), 47-61.

Kawabata, S., Niwa, M., & Kawai, H. (1973). The finite-deformation theory of plain-weave fabrics part I: the biaxial-deformation theory *Journal of the Textile Institute, 64*(1), 21-46.

Khoshbakht, M., Chowdhury, S., Seif, M., & Khashaba, U. (2009). Failure of woven composites under combined tension-bending loading. *Composite structures, 90*(3), 279-286.

Komeili. (2014). *Multi-scale characterization and modeling of shear-tension interaction in woven fabrics for composite forming and structural applications*. PhD Dessetation, University of British Columbia, Canada

Komeili, M. (2010). *Mechanical behavior of woven fabric composites under meso-level uncertainties: modeling and sensitivity analysis. m*ASc Dessetation, University of British Columbia, Canada

Komeili, M., & Milani, A. (2013). An elaboration on the shear characterization of dry woven fabrics using trellising tests. *Polymer Composites, 34*(3), 359-367.

Krstulovic-Opara, L., Klarin, B., Neves, P., & Domazet, Z. (2011). Thermal imaging and Thermoelastic Stress Analysis of impact damage of composite materials. *Engineering Failure Analysis, 18*(2), 713-719.

Launay, J., Hivet, G., Duong, A. V., & Boisse, P. (2008). Experimental analysis of the influence of tensions on in plane shear behaviour of woven composite reinforcements. *Composites Science and Technology, 68*(2), 506-515.

Lee, W., Byun, J.-H., Um, M.-K., Cao, J., Boisse, P., & LaMCoS, I.-L. (2009). *Coupled Non-orthogonal Constitutive Model For Woven Fabric Composites. t*he 17th International Conference on Composite Materials.

Lee, W., Um, M.-K., Byun, J.-H., Boisse, P., & Cao, J. (2010). Numerical study on thermo-stamping of woven fabric composites based on double-dome stretc. h forming. *International Journal of Material Forming, 3*(2), 1217-1227.

Lightfoot, J. S., Wisnom, M. R., & Potter, K. (2013a). Defects in woven preforms: Formation mechanisms and the effects of laminate design and layup protocol. *Composites Part A: Applied Science and Manufacturing, 51*, 99-107.

Lightfoot, J. S., Wisnom, M. R., & Potter, K. (2013h). A new mechanism for the formation of ply wrinkles due to shear between plies. *Composites Part A: Applied Science and Manufacturing, 49*, 139-147.

Long, A., Wilks, C., & Rudd, C. (2001). Experimental characterisation of the consolidation of a commingled glass/polypropylene composite. *Composites Science and Technology, 61*(11), 1591-1603.

Luo, R., Green, E., & Morrison, C. (2001). An approach to evaluate the impact damage initiation and propagation in composite plates. *Composites Part B: Engineering, 32*(6), 513-520.

Meola, C., & Carlomagno, G. M. (2010). Impact damage in GFRP: new insights with infrared thermography. *Composites Part A: Applied Science and Manufacturing, 41*(12), 1839-1847.

Mesogitis, T., Skordos, A., & Long, A. (2014). Uncertainty in the manufacturing of fibrous thermosetting composites: A review. *Composites Part A: Applied Science and Manufacturing, 57*, 67-75.

Milani, A., Nemes, J., Abeyaratne, R., & Holzapfel, G. A. (2007). A method for the approximation of non-uniform fiber misalignment in textile composites using picture frame test. *Composites Part A: Applied Science and Manufacturing, 38*(6), 1493-1501.

Mir, S. S., Hasan, M., Hasan, S. M. N., Hossain, M. J., & Nafsin, N. (2015). Effect of Chemical Treatment on the Properties of CoirFiber Reinforced Polypropylene and Polyethylene Composites. *Polymer Composites*. doi: DOI 10.1002/pc.23690

Mir, S. S., Hasan, S., Hossain, M. J., & Hasan, M. (2012). Chemical modification effect on the mechanical properties of coir fiber. *Engineering Journal, 16*(2), 73-84.

Mir, S. S., Nafsin, N., Hasan, M., Hasan, N., & Hassan, A. (2013). Improvement of physico-mechanical properties of coir-polypropylene biocomposites by fiber chemical treatment. *Materials & Design, 52*, 251-257.

Montgomery, D. C. (2008). *Design and Analysis of Experiments*: John Wiley & Sons.

Nosrat-Nezami, F., Gereke, T., Eberdt, C., & Cherif, C. (2014). Characterisation of the shear–tension coupling of carbon-fibre fabric under controlled membrane tensions for precise simulative predictions of industrial preforming processes. *Composites Part A: Applied Science and Manufacturing, 67*, 131-139.

Nunes, L., Paciornik, S., & d'Almeida, J. (2004). Evaluation of the damaged area of glass-fiber-reinforced epoxy-matrix composite materials submitted to ballistic impacts. *Composites Science and Technology, 64*(7), 945-954.

Patel, B., Acharya, S., & Mishra, D. (2011). Effect of stacking sequence on the erosive wear behavior of jute and juteglass fabric reinforced epoxy composite. *International Journal of Engineering, Science and Technology, 3*(1).

Peirce, F. T. (1937). 5—The geometry of cloth structure. *Journal of the Textile Institute Transactions, 28*(3), T45-T96.

Peng, X., & Cao, J. (2002). A dual homogenization and finite element approach for material characterization of textile composites. *Composites Part B: Engineering, 33*(1), 45-56.

Peng, X., & Cao, J. (2005). A continuum mechanics-based non-orthogonal constitutive model for woven composite fabrics. *Composites Part A: Applied Science and Manufacturing, 36*(6), 859-874.

Rashidi, A., Sultana, S., Crawford, B., DeWachter, M., & Milani, A. S. (2015). Towards wrinkling-free forming of woven composite materials. *2nd Annual Engineering Graduate Symposium*.

Ray, D., Bose, N. R., Mohanty, A. K., & Misra, M. (2007). Modification of the dynamic damping behaviour of jute/vinylester composites with latex interlayer. *Composites Part B: Engineering, 38*(3), 380-385.

Rowell, R. M., O'Dell, J., Basak, R., Sarkar, M., Rowell, R. M., Rowell, R. M., et al. (1997). *Applications of Jute in Resin Transber Molding.* Paper presented at the In: Proceedings, International seminar on jute and allied fibres: changing global scenario; Calcutta, India. Calcutta, India: Ijira Associaiton.

Rudd, C., Turner, M., Long, A., & Middleton, V. (1999). Tow placement studies for liquid composite molding. *Composites Part A: Applied Science and Manufacturing, 30*(9), 1105-1121.

Sargent, J., Chen, J., Sherwood, J., Cao, J., Boisse, P., Willem, A., . . . Mabrouki, T. (2010). Benchmark study of finite element models for simulating the thermostamping of woven-fabric reinforced composites. *International Journal of Material Forming, 3*(1), 683-686.

Sharma, S., Sutcliffe, M., & Chang, S. (2003). Characterisation of material properties for draping of dry woven composite material. *Composites Part A: Applied Science and Manufacturing, 34*(12), 1167-1175.

Sheahan, M. (2015, 2015). Special investigation: *Why Do Keel Failures Happen and What Can We Do To Prevent It*. Time Inc. (UK) Ltd. Yachting World

Shyr, T.-W., & Pan, Y.-H. (2003). Impact resistance and damage characteristics of composite laminates. *Composite Structures, 62*(2), 193-203.

Smith, J. R., & Vaidya, U. K. (2013). Processing Optimization of Deformed Plain Woven Thermoplastic Composites. *Applied Composite Materials, 20*(6), 1265-1272.

Spivak, S. (1966). The Behavior of Fabrics in Shear Part I: Instrumental Method and the Effect of Test Conditions. *Textile Research Journal, 36*(12), 1056-1063.

Spivak, S., & Treloar, L. (1967). The Behavior of Fabrics in Shear Part II: Heat-Set Nylon Monofil Fabrics and a New Dynamic Method for the Measurement of Fabric Loss Properties in Shear. *Textile Research Journal, 37*(12), 1038-1049.

Stig, F. (2009). An introduction to the mechanics of 3D-woven fibre reinforced composites.

Strong, A. B. (2008). *Fundamentals of Composites Manufacturing: Materials, Methods and Applications*. Society of Manufacturing Engineers.

Taha, I., Abdin, Y., & Ebeid, S. (2013). Comparison of picture frame and Bias-Extension tests for the characterization of shear behaviour in natural fibre woven fabrics. *Fibers and Polymers, 14*(2), 338-344.

Ullah, H., Harland, A. R., & Silberschmidt, V. V. (2012). Damage modelling in woven-fabric CFRP laminates under large-deflection bending. *Computational Materials Science, 64*, 130-135.

Willems, A., Lomov, S. V., Verpoest, I., & Vandepitte, D. (2008). Optical strain fields in shear and tensile testing of textile reinforcements. *Composites Science and Technology, 68*(3), 807-819.

Xue, P., Peng, X., & Cao, J. (2003). A non-orthogonal constitutive model for characterizing woven composites. *Composites Part A: Applied Science and Manufacturing, 34*(2), 183-193.

Yin, H., Peng, X., Du, T., & Guo, Z. (2014). Draping of plain woven carbon fabrics over a double-curvature mold. *Composites Science and Technology, 92*, 64-69.

Yu, T., Tao, X., & Xue, P. (2000). The energy-absorbing capacity of grid-domed textile composites. *Composites Science and Technology, 60*(5), 785-800.

Yu, W. R., Zampaloni, M., Pourboghrat, F., Chung, K., & Kang, T. J. (2003). Sheet hydroforming of woven FRT composites: non-orthogonal constitutive equation considering shear stiffness and undulation of woven structure. *Composite structures, 61*(4), 353-362.

Zampaloni, M. A., Pourboghrat, F., & Yu, W.-R. (2004). Stamp thermo-hydroforming: a new method for processing fiber-reinforced thermoplastic composite sheets. *Journal of Thermoplastic composite materials, 17*(1), 31-50.

Zhu, B., Yu, T., & Tao, X. (2007). An experimental study of in-plane large shear deformation of woven fabric composite. *Composites Science and Technology, 67*(2), 252-261.

Zhu, B., Yu, T., Teng, J., & Tao, X. (2008). Theoretical modeling of large shear deformation and wrinkling of plain woven composite. *Journal of Composite Materials,43*(2), 125-138.